IOP Publishing

RF-MEMS Technology for High-Performance Passives
(Second Edition)
5G applications and prospects for 6G
Jacopo Iannacci

Chapter 1

Introduction to MEMS and RF-MEMS: from the early days of microsystems to modern RF-MEMS passives

1.1 Introduction to semiconductor and microsystem technologies

Thinking of electronics and wondering about the intricacy of paths through which it has modified our habits, expectations and way of living in the last few decades, linking all these facts to the invention of the transistor (by John Bardeen, Walter Brattain and William Shockley at Bell Labs in 1947) seems quite spontaneous, both to people holding technical skills in semiconductor technologies, as well as to the general public. It is unequivocal that the transistor, as an elemental building block of any electronic circuit, was and is still today, the key element enabling the implementation of more complex and increasingly *smart* function/functionalities carried out by smaller, more integrated and less power-hungry devices.

Nonetheless, a quite critical consideration must be dragged into the spotlight before moving the discussion to the world of microsystems. In a rather effective attempt to reduce the complexity of a highly branched scenario, the transistor, according to a rather strict and classical definition, realises a limited set of main functions, as it can be exploited as a relay, i.e. an ON/OFF switch, as a varactor (i.e. variable capacitor), or as an amplifier, i.e. a device able to increase the amplitude of an electrical signal according to a certain proportionality law. None of these functions were enabled or *invented* by the transistor. The first electrically operated switch, or relay, is attributed to the American scientist Joseph Henry in 1835. Its development was driven by the advancement of telegraph technologies. On the other hand, the first thermionic valve for amplification purposes was invented by

doi:10.1088/978-0-7503-4199-8ch1

John Ambrose Fleming in 1904. Bearing in mind this scenario, it is straightforward that transistors and, more generally, semiconductor technologies, have been playing a key role in the development of electronic devices for decades, with no leverage on the novelty or complexity of the function implemented by a single device, with respect to its vacuum valve traditional counterpart. The actual key-enabling feature of semiconductor-based components is miniaturisation, closely linked to the ease of integration. Just to provide a simple visual interpretation of the latter concept, it is sufficient recalling that the computational capacity of a modern smartphone, 55 or 60 years ago, would have required a medium-size apartment full of thermionic valves, relays, wires and power cables, to be implemented. As a matter of fact, miniaturisation and integration enabled by semiconductor technologies, triggered a relentless trend in increasing the implemented complexity, counterbalanced by a moderate and, therefore, affordable spread in manufacturing and production costs, as well-framed by Moore's law [1]. As a matter of completeness, the latter states that with the advancement of technology, the number of transistors that can be integrated in a square inch of silicon doubles roughly every two years.

On the other hand, the development of microsystem technologies has followed a path that exhibits several factors in common with semiconductors, yet marking fundamental differences from such technologies for many other critical aspects.

Microsystems, which are universally referred to with the MEMS acronym (Micro-ElectroMechanical Systems), are millimetre/sub-millimetre devices, realising a certain transduction function between two (or more) distinct physical domains, among which the mechanical one is always involved. More simply, regardless of the specific function it is conceived for, a MEMS device always features tiny structural parts that move, bend, stretch, deform and/or contact together. These peculiarities make microsystem devices particularly suitable for the realisation of a very wide variety of micro-sized sensors and actuators.

Provided with these basic concepts, a few considerations around the differences and similarities of MEMS versus semiconductor technologies can now be developed. Commencing from the most obvious diversities, while semiconductor devices are active, i.e. able to amplify an electrical signal, MEMS are exclusively passive, i.e. can just attenuate an electrical signal. However, transistors do not feature any movable or deformable part, i.e. they do not exploit the mechanical/structural domain to realise transduction functions.

From a technological point of view, MEMS and semiconductors share most of the same micro-fabrication steps, as will be discussed later in more detail. Both feature selective deposition/removal of conductive/insulating thin-films by means of lithography, despite a few peculiar steps and sequences of fabrication that are typical of MEMS only.

Both MEMS and semiconductors pursue the concept of miniaturisation. However, if semiconductor devices, beyond down-scaling, implement in the electrical/electronic domain the multi-physical function of traditional components, MEMS often miniaturise classical objects, keeping their transduction across physical domains. To this regard, the example of the aforementioned relay is quite explanatory. The traditional electrically operated switch exploits the transduction

between the electrical and mechanical domain to realise the ON/OFF function. The transistor (when exploited as a switch) realises such a function entirely in the electrical/electronic domain. In contrast, a MEMS switch commutes between the ON/OFF state by coupling the mechanical and electrical domains, likewise the traditional device, despite the former being typically two or even three orders of magnitude smaller compared to the latter.

Also, importantly, the concept of miniaturisation is inflected in a radically diverse fashion when referring to semiconductor and MEMS devices. In the first case, as mentioned earlier, the trend in down-scaling has been continuous for decades. In order to build a more circumstanced idea, in Complementary Metal Oxide Semiconductor (CMOS) technology, the reference geometrical feature characterising the transistor is the channel length. In the mid-1980s such a length was around 4 μm, in the mid-1990s it was roughly 600 nm, in 2010 it reached 30 nm, while nowadays it is well below 20 nm [2]. This trend is, broadly speaking, addressed by the turn of phrase '*More Moore*', indicating the substantial hold of validity of Moore's law.

The concept of miniaturisation *played* by microsystem technologies, is completely different with respect to the aforementioned sketched scenario. First, there is no such thing as a trend in evolving technologies and processes in order to make the same MEMS device smaller, from one year to the next. Instead, a strong driver exists in implementing more and more functionalities, possibly bringing them from the macro- to the micro-world. In other words, if the transistor was the same device over a number of decades, benefiting from being smaller and becoming, in turn, faster, less power consuming, more integrated and so on, the MEMS is a miniaturised object that benefits from implementing more and/or diverse sensing/actuating/transducing functions, by means of a device roughly of the same size. Because of these characteristics, microsystems, as well as other non-standard technologies not mentioned here for brevity, are generally labelled by the turn of phrase '*More than Moore*' [3], indicating that their evolution through time does not follow Moore's law, as they cannot be standardised according to a development trend exclusively built upon the continual shrinking of dimensions.

Eventually, from a different perspective, the concept of miniaturisation is radically dissimilar in quantitative terms, as well, when referring to semiconductors rather than microsystems. While CMOS transistors, as mentioned before, are framed today in the range of nanometres, a MEMS sensor/actuator can span from a few micrometres (in-plane dimensions), to hundreds of micrometres, or even to a few millimetres. Therefore, if a MEMS switch is nearly invisible to the naked eye when compared to a traditional relay, it is massive when placed beside a CMOS transistor.

In the following subsections, a few key considerations will be developed around the early days of MEMS, the most diffused micro-fabrication techniques and their market applications. Such concepts will help one to understand the core topic of this work, which will be introduced immediately after, i.e. MEMS for Radio Frequency applications, universally known as RF-MEMS.

1.1.1 The genesis of MEMS

As already discussed, the non-standard underlying peculiarity of microsystems with respect to semiconductors has emerged. Due to this reason, development of MEMS as a whole has not followed a well-established path, making it difficult to determine an exact point in time corresponding to the conception of microsystems.

From the point of view of technology, the key fabrication steps developed concomitant with the growth of semiconductor technologies starting in the 1950s. Nonetheless, the exploitation of such techniques aimed towards the manufacturing of microsystems commenced later, in the early 1970s. The advancement of silicon-based semiconductor technology motivated the scientific community to investigate, beside critical aspects related to the electrical/electronic characteristics, the mechanical properties of the materials involved in the manufacturing of semiconductors. In this regard, significant contributions can be found, for instance, in the valuable work of several authors concerning the mechanical properties of both bulk materials [4] and deposited thin-layers [5–7], dating from the mid-1950s to mid-1960s. Nevertheless, the exploitation of such techniques aimed towards the manufacturing of micro-devices with movable parts and membranes emerged later, in the period from the second half of the 1970s to the beginning of the 1980s.

Examples around how to exploit anisotropic etching to obtain a variety of 3D suspended structures from a silicon substrate are provided in [8]. Such techniques, together with those typically exploited for the fabrication of transistors and Integrated Circuits (ICs), led to the realisation of miniaturised pressure sensors [9], accelerometers [10, 11], switches [12, 13], and other devices for various applications, such as in the optical and biomedical fields. A remarkable article summarising the state-of-the-art microsystem technologies, and providing a comprehensive outlook around diverse applications, was authored by Petersen [14] at the beginning of the 1980s.

Nonetheless, it was with the further maturation of the surface micromachining fabrication technique [15] that the development of microsystems started to receive a significant boost, leading to the concepts of MEMS sensors and actuators as we know them today. A relevant contribution is represented by the work of Howe and Muller [16] in 1983, in which micro-cantilevers and double-supported beams were realised in polycrystalline silicon, and released suspended above the substrate, via silicon oxide utilised as a sacrificial layer. Since then, a wide variety of MEMS-based sensors, actuators, and various mechanisms, like gears and micro-motors, have been developed, tested, and reported in the literature [17–19].

In addition to what has just been outlined, another significant element of diversity emerges between semiconductor and microsystem technologies. The integration of transistors in silicon-based substrates on one side, and the novelty of the electrical/electronic properties of semiconductor materials, on the other hand, stimulated for decades the aggregation and strengthening of a distinct and unprecedented multi-disciplinary domain of science. Within it, classical physics and chemistry converged, mainly driven by the development of technology, together with mathematics and electrical techniques necessary for the functional understanding of novel devices.

This resulted in boosting the development of the electronics discipline, which today encompasses, at the same time, computer-based codes for designing circuits and systems, as well as quantum theory to describe the physical behaviour of state-of-the-art semiconductor devices.

On a different plane, microsystems did not prosper as a well-structured discipline in the beginning. Essentially, the possibility to realise mechanical micro-devices was seen in the early days as a sort of side-branch of the more and more standardised semiconductors manufacturing stream. As the small scientific community working in the MEMS field was mainly involved in the development of transistors and active devices, a consolidated background in mechanics and structural mechanics was essentially missing. However, the community of mechanical/structural engineers was neither particularly interested in, nor even fascinated by, the idea of bringing part of their expertise *down to* the micro-world, especially from the mid-1950s to the 1960s, when the massive development of modern aircraft was driving research. It was only much later, roughly from the first half of the 1990s, that MEMS started to emerge as a self-standing discipline, where basic knowledge of physics, chemistry, electronics and fabrication started to be blended together with structural mechanics, electro-mechanics and functional reliability. Such a statement is corroborated by the fact that in those years the first books, scientific journals and international conferences explicitly focused on microsystems started to emerge, supported by the growth of a sectorial community of researchers, designers, engineers and developers.

1.1.2 Micro-fabrication technology platforms

The manufacturing of semiconductor components, like transistors, consists in a sequence of steps in which different doses of dopant materials are selectively implanted/diffused within a substrate (typically silicon) to obtain (locally) certain electrical properties. The same implantation/diffusion, or alternatively the digging of deep trenches, can be performed to enhance isolation and reduce the cross-talk between adjacent devices. In addition, conductive and insulating layers are selectively deposited/grown, or deposited/grown everywhere and then selectively removed, in order to redistribute the electrical signals, from the intrinsic devices to the external world. The most important steps in the manufacturing of ICs are ion implantation, diffusion, epitaxial growth, chemical vapour deposition/physical vapour deposition and their variations, wet and dry-etching, sputtering, evaporation and electrodeposition of metals. The selection of the areas that have to undergo one or more of the previously listed steps, is achieved by means of lithography [20]. A typical cross-section view of CMOS transistors is depicted by the schematic in figure 1.1.

Looking at the cross section, a couple of considerations must be developed. First, the intrinsic device is *made into silicon*, where differently doped areas (with diverse electrical/electronic properties) are obtained through the aforementioned fabrication steps. Second, the transistors themselves are very small, while the metal and insulating layers stacked above them, necessary to redistribute the electrical signals from each transistor terminal to the external world, can be several times the size of

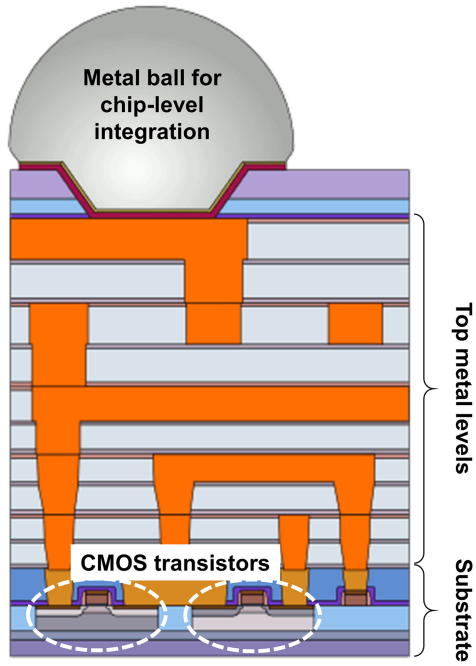

Figure 1.1. Schematic cross section of CMOS transistors. Image from [21] CC BY 3.0.

the semiconductor intrinsic devices. In figure 1.1 the stack is completed at the top by a metal ball, necessary for chip-level integration, i.e. for mounting/interfacing the CMOS circuit into a more complex system or subsystem.

Microsystems, as mentioned earlier, are manufactured relying (for the most part) on the fabrication steps commonly utilised in the processing of semiconductors, even though they are arranged according to different sequences. Despite the fact that MEMS technology is not highly standardised like CMOS, it is possible to identify two distinct processing streams, which are the most diffused, both in the research and commercial production of microsystems. For the sake of completeness, there also exist highly customised technology platforms strongly oriented to the manufacturing of MEMS. Such solutions enable one to achieve very high aspect ratios and extremely precise geometrical features. Nonetheless, their pronounced customisation makes them diverse from CMOS-like processes, resulting in significantly higher costs and more articulated issues in terms of integration with other (incompatible) technologies. Because of their suitability for niche applications, these solutions will not be discussed further in this work. However, it is worth mentioning that the Lithography, Electroplating, and Moulding process (in German, *Lithographie, Galvanoformung, Abformung—LIGA*), is one of the best-known highly customised technologies for the manufacturing of MEMS [22, 23].

Coming back to the most common aforementioned MEMS fabrication flows, they are substantially two: *surface micromachining* and *bulk micromachining*.

In surface micromachining processes, the substrate (silicon or other materials) is used as a sort of *ground floor* plane. All the selective depositions/removals of the conductive/insulating layers are performed above the substrate, through the techniques and steps mentioned above. From a conceptual point of view, a surface micromachining process is not crucially different from the above-CMOS stacking of layers depicted in figure 1.1. The substantial addition of a MEMS surface micromachining process is that membranes and movable parts need to be suspended in air. To do so, a temporary layer is necessary to support mechanically the micro-membranes during their manufacturing (e.g. through electrodeposition or sputtering). Afterwards, it has to be removed via an etching step, in order to release the so-called air gaps, i.e. membranes suspended above the substrate and, therefore, free to move. Such temporary support is referred to as a sacrificial layer, and it can be a photoresist material or a thin-film deposited during processing [24, 25]. Accordingly, it can be stated that in surface micromachining, MEMS devices are *made above silicon*.

A typical schematic cross section of a MEMS surface micromachining process is reported in figure 1.2(a), while a microphotograph of physical gold-based MEMS devices, manufactured with such a technology solution [26], is shown in figure 1.2(b).

In this example, the silicon substrate is 625 μm thick, the air gaps are around 3 μm, while the suspended gold membrane's thickness ranges between 2 and 5 μm. Each of the MEMS in figure 1.2(b) has in-plane dimensions of 2 mm by 0.7 mm.

In bulk micromachining processes, the substrate itself (typically, but not limited to, silicon) is exploited for the realisation of the structural parts of MEMS. By means of performing selective etching (removal) of substrate-specific regions, e.g. Tetramethylammonium Hydroxide (TMAH)-based wet-etching [27] or Deep Reactive Ion Etching (DRIE) dry-etching, thin and deformable membranes are released [28]. Still keeping the same idiomatic expression as above, it can be stated that in bulk micromachining, MEMS devices are *made of silicon*. In light of the discussion developed up to this point, bulk micromachining of MEMS deviates from standard semiconductor processes more than surface micromachining does.

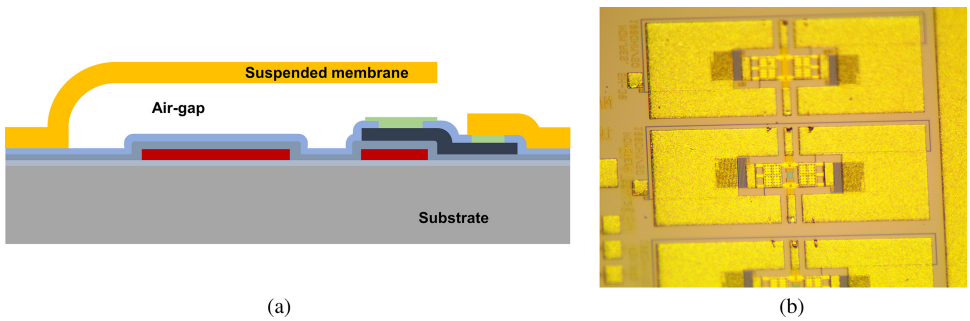

(a) (b)

Figure 1.2. (a) Schematic cross section of a typical surface micromachining MEMS process. (b) Microphotograph of physical MEMS devices realised by means of a surface micromachining process based on gold [26].

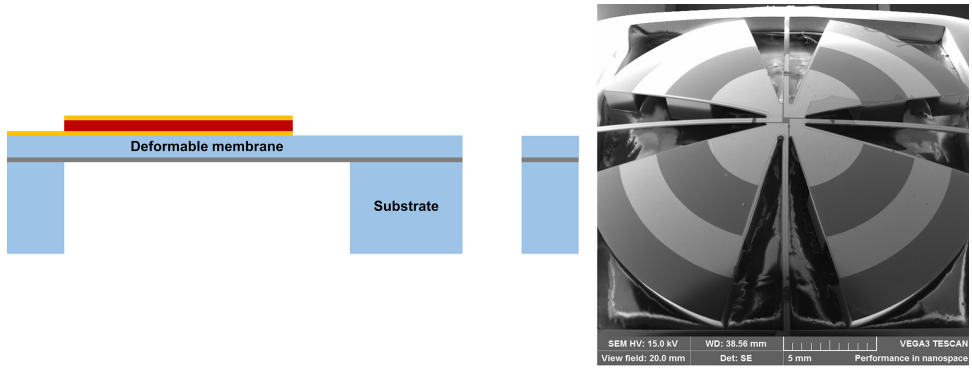

(a) (b)

Figure 1.3. (a) Schematic cross section of a typical bulk micromachining MEMS process. (b) SEM image of physical MEMS for Energy Harvesting (EH-MEMS) devices realised by means of a bulk micromachining process based on silicon [29].

If the latter solution is, for simple MEMS structures, an extension of the above-CMOS stacking of layers, in the former it is silicon (and its mechanical properties) that is to be exploited as a structural material. It is straightforward that silicon mechanical structures of MEMS devices fabricated through bulk micromachining can be completed by selective deposition of conductive/insulating layers, in order to deploy proper electrodes and feeding lines to enable electromechanical transduction.

A typical schematic cross section of a MEMS bulk micromachining process is reported in figure 1.3(a), while a Scanning Electron Microscopy (SEM) image of a physical silicon-based MEMS for Energy Harvesting (EH-MEMS) realised with such a technology [29] is shown in figure 1.3(b).

In the reported example, the initial silicon substrate is 390 μm thick, while, after the etching step, the silicon deformable membranes are 20 μm thick. The diameter of the suspended mechanical resonator in figure 1.3(b) is 8 mm.

1.1.3 Applications of MEMS sensors and actuators

To complete the overview of microsystem technologies on a general perspective, and before embarking on an in-depth discussion around RF-MEMS, a few references and examples of MEMS sensors' and actuators' market applications are going to be briefly provided.

In the first place, it should be highlighted that, if microsystem technologies started to develop in the 1970s (as discussed earlier), the first MEMS-based commercial product, namely, a surface micromachined accelerometer by Analog Devices [30], only showed up in the early 1990s, nearly two decades later. The rationale beneath the lengthy time-to-market characterising the early exploitation of MEMS in the field of sensors and actuators, is a sizable mosaic composed of numerous tiles, featuring crucial pivots, like reliability [31], packaging, integration, as well as costs

and, last but not least, market readiness. These aspects will be treated with deeper specificity later, when discussing RF-MEMS.

Starting from the first commercial accelerometer mentioned in [30], MEMS-based sensors and actuators started to spread into diverse systems and devices, securing their presence in significant market segments. Accelerometers themselves, for instance, became, through the 1990s, a de facto standard in the automotive sector, being employed as deceleration sensors activating the inflation of airbags in case of car crashes [32]. Concerning microsystem-based actuators, another successful exploitation of MEMS technology is related to micro-mirrors and, in particular, to their arrangement in high-density matrices of individual micro-devices. MEMS micro-mirrors have been commercially employed since the second half of the 1990s to form optical images on projectors lenses, as well as on movie theatre screens. In this regard, Digital Micromirror Devices (DMDs) are well-known, and named in such a fashion because they are not controlled in an analogue way, but rather with two-state (ON/OFF) driving signals [33, 34].

In more recent years, MEMS accelerometers and gyroscopes, i.e. inertial devices sensitive to rotations around axes and to gravity, experienced a boost in terms of market volumes, significantly larger than traditional applications in the automotive sector. In the last decade, with the emergence of home video game consoles interacting with human motion, and later with the massive spread of smartphones and tablets, MEMS-based Inertial Measurement Units (IMUs) became standard components provided by a wide variety of Original Equipment Manufacturers (OEMs) [35].

Just to mention a few other classes of devices, MEMS are spreading in the switching/multiplexing of optical signals (actuators), miniaturised microphones (sensors) and, despite not being fully mature yet, loudspeakers (actuators), Energy Harvesters (EH) for environmental sources (sensors), pressure/gas/temperature sensors, strain gauges/deformation sensors, and so on. The targeted fields of applications are quite diverse, as they range from automotive to consumer electronics, as well as from space/defence to the medical/health sector.

Eventually, it can be stated with a certain confidence that trends in the exploitation of MEMS will keep ramping up in the years to come. The crucial paradigms of the Internet of Things (IoT) [36] and of the Internet of Everything (IoE) will demand for the availability of smaller, cheaper, less power hungry, multi-functional and more specialised sensors and actuators, to be integrated in increasing numbers within Smart-Cities, -Buildings, -Devices, -Factories, -Cars, -Objects, as well as the human body, e.g. through Body Area Networks (BANs).

1.2 Introduction to RF-MEMS

Bearing in mind the scenario previously described, the investigation of microsystem technologies for the realisation of RF passive components is more recent. The first scientific contributions relating to the exploitation of MEMS-like technology steps for RF passives started to appear in the landscape in the early 1990s, i.e. while MEMS accelerometers were establishing themselves as valuable commercial

products. However, early examples of actual RF-MEMS devices only started to populate the scientific literature in the second half of the 1990s.

At an early stage, miniaturisation of microwave and millimetre-wave transmission lines, and their implementation in micromachining technologies based on silicon, emerged as a quite promising research field [37], thanks to the outstanding performance figures in terms of their low loss and compactness compared to traditional solutions [38]. The possibility of integrating fixed RF signal manipulation functions, e.g. through the realisation of stubs [39], appeared as an additional strength of silicon-based waveguides. Among the various families of transmission line configurations available, and well-known for decades [40], micro-fabrication technologies are particularly suited for planar devices. Therefore, most of the attention and interest concerning their miniaturisation was around the Coplanar Waveguide (CPW) and microstrip implementations of transmission lines.

Given these premises, the fundamentals of the aforementioned waveguide configurations are going to be synthetically recalled here. A 3D schematic view of a CPW and microstrip configuration is shown in figure 1.4(a) and figure 1.4(b), respectively. In the former, a central metallisation acts as the RF signal line, while two wider metallised patches are meant to be reference ground planes for the travelling RF signal. The central line and ground planes are separated by a gap, and all the metal layers lie on the same side of the substrate [41]. As the RF signal

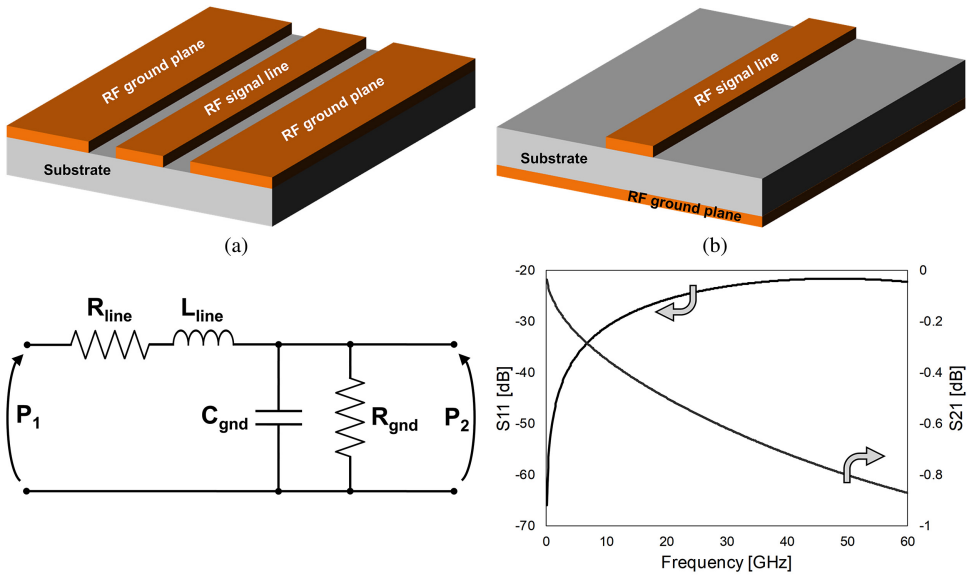

Figure 1.4. (a) Schematic 3D view of a transmission line in Coplanar Waveguide (CPW) configuration. (b) Schematic 3D view of a transmission line in a microstrip configuration. (c) Equivalent lumped element network of a CPW/microstrip line. P_1 and P_2 are the input/output terminations, respectively. (d) Typical S-parameters versus frequency characteristic of a CPW/microstrip line concerning reflection (S11 at P_1) and transmission through the line (S21 at P_2).

propagates along the waveguide, the electromagnetic field is confined between the central line and the ground planes, partially through the dielectric material underneath the metal layers, and partially through the air above them. Very often, a thin insulating layer is deposited on the substrate prior to the electroplating/evaporation of the CPW itself. This helps to reduce losses to the substrate. In the microstrip configuration, instead, the RF signal line is placed on top of the substrate, while a unique reference ground plane is metallised on the opposite face of the wafer. In this case, as the RF signal propagates along the waveguide, the electromagnetic field is mainly confined within the substrate, between the two metal layers (signal line and ground plane).

A basic lumped element network description useful to model the RF behaviour of CPWs and microstrip lines is proposed in [42] and depicted in figure 1.4(c). Across the waveguide input and output ports P_1 and P_2, a resistance and inductance are inserted, representing the series resistive (R_{line}) and inductive (L_{line}) contributions of the metal RF line, respectively. On the other hand, the shunt-to-ground capacitance and resistance model the capacitive coupling (C_{gnd}) and the resistive losses (R_{gnd}) between the RF line and the ground plane/s, respectively, through the substrate material and across air. The values of the resistive and reactive components in figure 1.4(c) are correlated to the physical properties of the transmission line, and can be parameterised in quite a straightforward fashion, in order to account for the most relevant geometrical features of the CPW or microstrip waveguide, like the length, gap, substrate thickness, and so on [43].

The RF behaviour of a typical CPW/microstrip line in terms of scattering parameters (S-parameters) versus frequency [42] is shown in figure 1.4(d). The curves result from the simulation of a CPW by means of a Finite Element Method (FEM) software tool, in the frequency range from DC to 60 GHz. The S11 parameter indicates the fraction of RF signal reflected at the input port of the CPW. Given that it is small on the whole frequency range (better than −22 dB), most of the RF signal flows into the waveguide. The S11 and S22 (reflection at the input and output ports, respectively) are particularly suited to provide an indication of matching between the characteristic impedance of the RF source and of the transmission line. Low values of S11/S22 mean good impedance matching, indeed. The S21 parameter indicates the amount of RF power reaching the output port of the CPW (transmission). Since its worst value (around −0.9 dB) is quite close to 0 dB (i.e. ideal zero losses), the attenuation of the RF signal introduced across the waveguide is limited overall across the analysed frequency span.

Beside the exploitation of a typical surface micromachining step, like selective deposition of thin metal films, additional techniques have begun to be explored with the aim of improving the RF characteristics of miniaturised CPWs and microstrip lines. For instance, shallow tranches were etched in the gap between the RF signal line and the reference ground planes, in order to reduce the losses due to penetration of the electromagnetic field through the substrate, as reported in [44]. In other examples, bulk micromachining was used to remove most parts of the silicon substrate, yielding CPWs suspended above a thin membrane, resulting in a significant reduction of losses and parasitic coupling effects, as discussed in [45, 46].

Shortly after, MEMS technology began to be demonstrated for the realisation of micro-switches [47] and variable capacitors (varactors) [48], as well as tunable filters [49], resonators [49] and programmable phase shifters [50], thus starting to address the crucial feature of reconfigurability. All these aspects are going to be discussed in more detail through the following subsections.

1.2.1 Switches and simple passives in RF-MEMS technology

Based upon the discussion developed in the above sections, it is straightforward that the reconfigurability of a certain microsystem device can be enabled by inclusion of fabrication steps purposely conceived for such a target. Recalling what was mentioned at the beginning, in a case where the surface micromachining process is used, such a specific step is the exploitation of a sacrificial layer, meant to define and then release suspended structures. In contrast, when dealing with bulk micromachining, the MEMS structure has to be properly etched in order to be released and made free to move.

A few fundamental notions concerning actuation mechanisms are going to be recalled in the following pages. Subsequently, examples of physical RF-MEMS basic passive components will be discussed.

A brief review of actuation mechanisms

From a functional point of view, multi-physical coupling through which mechanical behaviour of movable RF-MEMS parts is controlled (and their characteristics reconfigured) can take place basically according to four different actuation principles: electrostatic, electromagnetic, piezoelectric, and thermoelectric [51]. These different mechanisms are going to be briefly explained.

- ***Electrostatic actuation***. Two electrodes, one fixed and one movable, are necessary, and they must face each other, as in a typical parallel plate capacitance configuration. When a voltage drop is applied across the two faces, the electrostatic attraction force makes the movable electrode approach the fixed one. Above a certain biasing threshold, called 'pull-in voltage', the movable part collapses onto the underlying fixed one. Figure 1.5 shows a

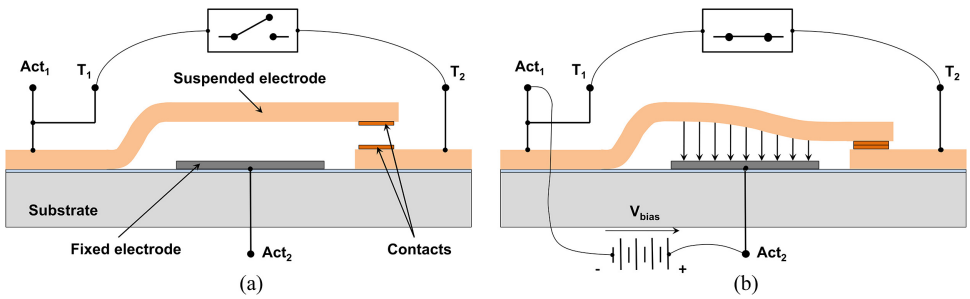

Figure 1.5. (a) Schematic cross section of a cantilevered MEMS series ohmic switch controlled through the electrostatic principle, in the rest position (OFF state). (b) Schematic cross section of the actuated or pulled-in position (ON state), when a bias voltage is imposed between the fixed and the floating electrode.

schematic cross section of an electrostatically controlled cantilever MEMS series ohmic switch [52].

In more detail, figure 1.5(a) reports the cantilever switch in its rest position (no bias imposed). In the latter condition, the input/output terminals (T_1 and T_2) are disconnected, and the micro-relay is in the OFF state, as indicated by the switch symbol above the schematic. However, when a voltage V_{bias} larger than the pull-in threshold is imposed between the movable (Act_1) and fixed (Act_2) electrodes, the contact between T_1 and T_2 is closed, and the switch commutes to the ON state, as indicated in figure 1.5(b).

- ***Electromagnetic actuation***. The suspended MEMS membrane has either to be made of or coated with a ferromagnetic material in order to be sensitive to magnetic field variations. In addition, a magnetic field must be generated by driving a current across a coil, and the former has to surround the deformable membrane. In such a way, when a bias current is imposed, the MEMS part deforms due to the interaction between the magnetic-sensitive material and the external induced magnetic field [53]. A schematic cross section of a cantilever series ohmic MEMS switch driven through electromagnetic actuation is reported in figure 1.6.

In particular, figure 1.6(a) shows a schematic of a MEMS switch in the rest position, i.e. when no bias current is driven across the terminations Act_1 and Act_2. In this case, high impedance is detected between the switch input and output ports, named T_1 and T_2, and the switch results in being OPEN (OFF state). On the other hand, when a current is driven through the coil, a magnetic field builds around the MEMS and the latter deforms until reaching pull-in, as shown in figure 1.6(b). In such a circumstance, the impedance between T_1 and T_2 commutes to a very low value, due to the physical contact between the two metal patches under the cantilever free end, and the switch is CLOSED (ON state).

- ***Piezoelectric actuation***. The suspended MEMS membrane must be covered/coated by/with a thin-film of material holding piezoelectric properties. As

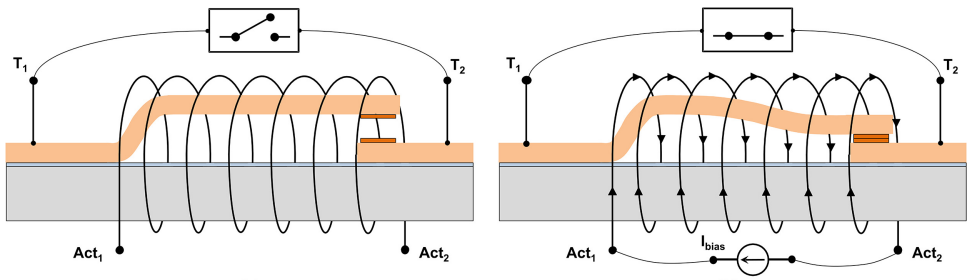

Figure 1.6. (a) Schematic cross section of a cantilevered MEMS series ohmic switch controlled through the electromagnetic principle, in the rest position (OFF state). (b) Schematic cross section of the actuated or pulled-in position (ON state) when a bias current is driven through the coil that induces a magnetic field around the movable MEMS membrane (the latter coated with a ferroelectric material).

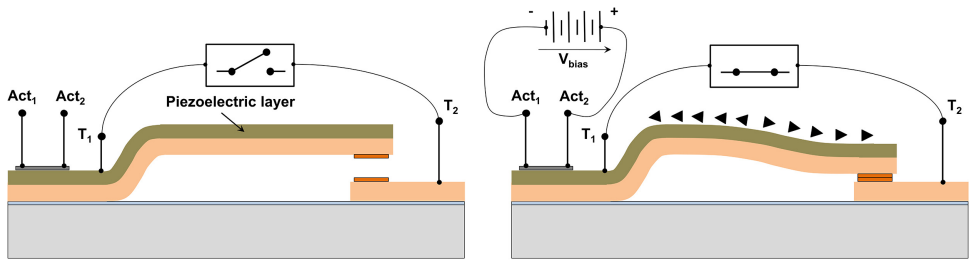

Figure 1.7. (a) Schematic cross section of a cantilevered MEMS series ohmic switch controlled through the piezoelectric principle, in the rest position (OFF state). (b) Schematic cross section of the actuated or pulled-in position (ON state) when the piezoelectric film is subjected to a bias voltage.

known, piezoelectric materials, which fundamentally behave electrically as insulators, exhibit the property of deforming/expanding when subjected to a voltage drop across their opposite faces [54]. As the piezoelectric thin-film is typically patterned above the MEMS structural part (made of bulk silicon of other supporting material), its expansion due to the piezoelectric effect results in a downward (momentum-induced) displacement [55]. A schematic cross section of a cantilever series ohmic MEMS switch driven through piezoelectric actuation is shown in figure 1.7.

In the MEMS rest position, depicted in figure 1.7(a), the switch is OPEN (OFF state). By contrast, when a bias voltage is imposed between Act_1 and Act_2, the piezoelectric material expands and induces commutation of the micro-relay to the CLOSED condition (ON state) between T_1 and T_2, as shown schematically in figure 1.7(b).

- ***Thermoelectric actuation***. In this case, the thermal expansion property of materials is exploited to drive the MEMS movable part(s). An electric current is driven across the suspended membrane that heats up due to its resistance and, therefore, expands because of the temperature increase [56]. Alternatively, thermal expansion of the suspended membrane can also be induced generating the heat not directly into the MEMS part itself, but, for instance, embedding micro-heaters underneath the device. This latter solution makes it possible to use materials with much higher resistivity (like polycrystalline silicon) than metals typically employed for the structural parts of microsystems (like gold, copper, aluminium, etc). Therefore, it is sufficient to drive a fairly low current through the heater in order to obtain the desired increase of temperature [57, 58]. A schematic cross section of a cantilever series ohmic MEMS switch driven through thermoelectric actuation is shown in figure 1.8.

In more detail, figure 1.8(a) reports the switch in the rest, i.e. OPEN, position (OFF state). In contrast, when a bias voltage is imposed across Act_1 and Act_2, a

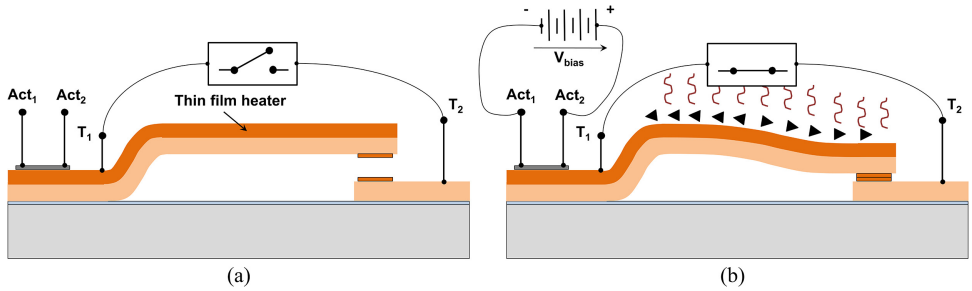

Figure 1.8. (a) Schematic cross section of a cantilevered MEMS series ohmic switch controlled through the thermoelectric principle, in the rest position (OFF state). (b) Schematic cross section of the actuated or pulled-in position (ON state) when a bias current is driven across the suspended membrane, causing the heating and the subsequent thermal expansion of the MEMS structure.

current is driven through the MEMS, and the generated heat brings commutation of the micro-relay in the CLOSED position (ON state), shown schematically in figure 1.8(b).

Among these reviewed mechanisms, electrostatic actuation is certainly the most commonly used for controlling RF-MEMS devices. There are multiple motivations for this choice. One reason being that, at the technology level, electrostatic actuation does not require the deposition of exotic materials, e.g. with piezoelectric or ferromagnetic properties, therefore easing the manufacturing process and also limiting the costs. Furthermore, at the operation level, this kind of driving method does not induce irreversible changes in the mechanical properties of the MEMS, which may happen, for instance, with thermoelectric actuation. Additionally, the effort in terms of energy employed to control MEMS devices is lower if compared with other methods, among which thermoelectric and electromagnetic actuations are definitely the most power hungry. As in electrostatically controlled MEMS, the physical contact between the movable and fixed electrodes must be avoided to prevent a short-circuit, so that no current flows through the device, leading to virtually zero power consumption of the micro-relay, in both ON/OFF configurations. In fact, small current leakages are always present along the DC biasing lines. Nonetheless, they lead in any case to very limited amounts of power necessary to drive the MEMS. In addition, the electrostatic actuation of MEMS will be often referenced in the practical examples shown later in this work. In light of all these considerations, further technical discussion around electrostatics is briefly reported below.

An electrostatically controlled MEMS device can be effectively represented as a parallel plate capacitor, with one fixed and one movable plate, as discussed in [59] and reported in figure 1.9.

A one Degree Of Freedom (1 DoF) parallel plate schematic is shown in figure 1.9(a). The lower plate is mechanically constrained, while the upper one is joined to a mechanical spring whose elastic constant is k. The spring allows displacement along the vertical x axis. The area of both plates is A, while their

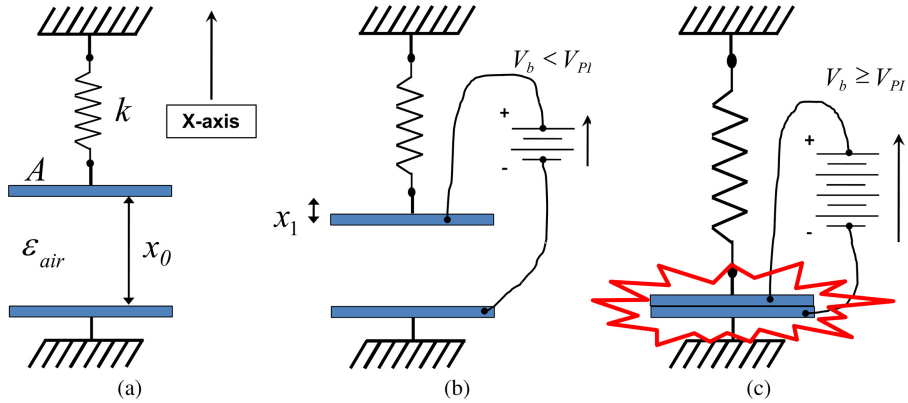

Figure 1.9. (a) Schematisation of an electrostatically controlled MEMS device as a parallel plate capacitor, with one plate fixed and the other movable, when no bias voltage is applied ($V_b = 0$). (b) Displaced movable plate when a bias voltage lower than the pull-in threshold ($V_b < V_{PI}$) is imposed across the two plates. (c) Collapsed (pulled-in) movable plate when a bias voltage equal or larger than the pull-in threshold ($V_b \geq V_{PI}$) is imposed across the two plates.

initial distance is x_0. They are immersed in air (dielectric constant ε_{air}) and the effects of gravity on the upper plate and spring can be neglected.

When a biasing voltage V_b is imposed across the two plates, and when it is below the pull-in threshold ($V_b < V_{PI}$), the situation is reported in figure 1.9(b). Due to electrostatic interaction, the upper plate moves downward of x_1. The electrostatic attraction force F_{el} is expressed by equation (1.1):

$$F_{el} = \frac{1}{2}\frac{\varepsilon_{air}A}{(x_0 - x_1)^2}V_b^2 = \frac{1}{2}\frac{C(x)V_b^2}{(x_0 - x_1)} \tag{1.1}$$

At the same time, still referring to figure 1.9(b), the spring elongates of x_1, giving rise to the mechanical restoring force F_{mech}, opposed to F_{el}, expressed by Hooke's law as follows:

$$F_{mech} = -kx_1 \tag{1.2}$$

Such a situation refers to an equilibrium condition since, given a certain $V_b < V_{PI}$, F_{mech} counteracts F_{el}, and the movable plate remains steadily at a distance equal to x_0–x_1 from the underlying fixed electrode. Nonetheless, it should be noted that, while F_{mech} linearly depends on the distance between the plates, commonly referred to as the air gap, F_{el} depends on its square value. By solving the system of equations (1.1) and (1.2) with respect to the voltage, it is possible to derive the pull-in voltage (V_{PI}), expressed as follows:

$$V_{PI} = \sqrt{\frac{8}{27}\frac{kx_0^3}{\varepsilon_{air}A}} \tag{1.3}$$

Such a threshold bias level makes the movable plate collapse abruptly above the underlying fixed plate, as reported in figure 1.9(c). In other words, the vertical displacement of the upper plate towards the lower one can be controlled in an analogue fashion, as long as $V_b < V_{PI}$, corresponding to one-third of the initial air gap (x_0). From a physical point of view, V_{PI} is the limiting level for which F_{el} becomes too large to be counteracted by F_{mech}, and the system becomes unstable. As figure 1.9(c) is a simplified schematic, no insulating layer is indicated between the two collapsed plates. In fact, physical contact must be avoided when pull-in occurs, as it would short-circuit the two plates. For this reason, in real MEMS, a thin insulating layer (of thickness t_{ins}) is always deposited above the underlying fixed electrode. Alternatively, or in conjunction with such a layer, electrically floating stoppers (i.e. elevated posts) can also be deployed, in order to allow clearance between the pulled-in electrodes. Once pull-in takes place, if the bias voltage is progressively decreased, there exists another threshold value corresponding to the release (detaching) of the collapsed plate, named pull-out voltage (V_{PO}), which is expressed as follows:

$$V_{PO} = t_{ins}\sqrt{\frac{2kx_0}{\varepsilon_{ins}A}} \tag{1.4}$$

As mentioned before, since F_{el} depends on the square of the imposed voltage, V_{PO} is typically much smaller than V_{PI}. This means that the pull-in/pull-out (actuation/release) characteristic of an electrostatically controlled MEMS device exhibits a certain hysteresis, as clearly emerges from the plot in figure 1.10.

When decreasing the bias voltage, right after pull-out occurs, the vertical displacement characteristic reconnects with the one previously obtained for increasing V_b levels (of course lower than V_{PI}). Eventually, since F_{el} depends on the square of the imposed voltage, as indicated by equation (1.1), the pull-in/pull-out

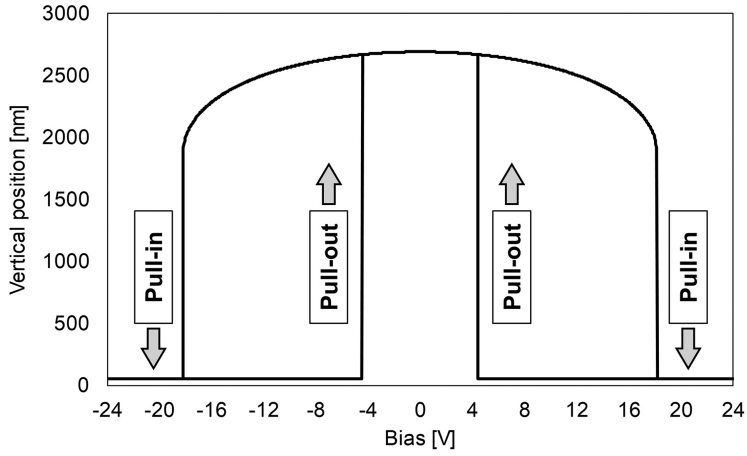

Figure 1.10. Typical pull-in/pull-out characteristic, i.e. vertical displacement versus imposed bias, of an electrostatically controlled MEMS device.

characteristic does not change if positive or negative bias levels are applied. This characteristic is straightforward when looking at the plot in figure 1.10, which is symmetric with respect to the 0 V vertical axis.

Next, examples of physical RF-MEMS simple components discussed in the literature are going to be reported. For the sake of homogeneity in explanation, all the photographs of the physical samples shown in the next pages refer to electrostatically controlled RF-MEMS devices realised in the same surface micromachining technology platform, detailed in [60, 61]. In all of the following microphotographs, the MEMS devices and CPWs/microstrip lines are made of electrodeposited gold, with a thickness ranging between 2 and 5 μm. The thickness of the sacrificial layer and, therefore, of the air gaps, is always around 3 μm. A buried polycrystalline silicon layer (high resistivity) is exploited to realise fixed DC biasing electrodes, underneath the suspended MEMS membranes. Moreover, an additional aluminium buried layer (low resistivity) is employed to implement RF signal underpasses and contact areas. A schematic cross section of this technology was previously reported in figure 1.2(a). Nonetheless, examples referring to other technologies discussed in the literature will also be reported.

RF-MEMS ohmic and capacitive switches

Briefly summarising what was discussed earlier, micro-fabrication technologies enable the manufacturing of miniaturised waveguides, mainly in CPW and microstrip configuration. By adding MEMS-specific fabrication steps, it is possible to realise suspended thin membranes, which can be driven/controlled according to different transduction mechanisms. The focus of this work is on electrostatically controlled RF-MEMS. Therefore, most of the examples that are going to be discussed in the following will refer to such a type of multiphysics coupling.

Having said that, the fundamental building block that enables the reconfigurability of RF-MEMS is represented by the micro-relay (or switch). The switching function, despite being based on a two-state (OPEN/CLOSED) configuration, can be implemented according to different fashions, as it can be ohmic or capacitive, as well as series or shunt [62]. Of course, these listed features can be paired together according to all of the possible combinations. As representative examples, series ohmic and shunt capacitive RF-MEMS switches are going to be discussed in detail.

Figure 1.11 shows a microphotograph of a cantilevered RF-MEMS series ohmic switch, electrostatically controlled in CPW configuration.

The movable membrane is placed in-line on the RF signal path. It is anchored on one side and free to move on the other, as shown in the close-up in figure 1.11(b). As a contact area is placed underneath the suspended tip, metal-to-metal contact is established when the MEMS is pulled-in. Therefore, the switch is OPEN when the MEMS is OFF (rest position), while it is CLOSED when the MEMS is ON (pulled-in), as reported in the simplified schematics in figure 1.12(a) and figure 1.12(b), respectively. The cantilever exhibits measured pull-in and pull-out voltages of 65 and 50 V, respectively. The experimental RF behaviour in terms of the S-parameters is also reported in figure 1.12, and refers to a frequency range from DC up to 40 GHz. In particular, figure 1.12(c) shows the reflection (S11) and isolation (S21) when the

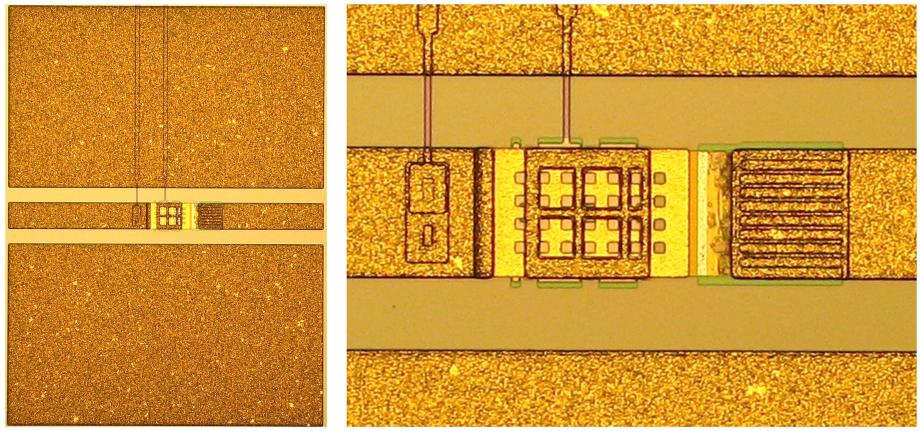

(a) (b)

Figure 1.11. (a) Microphotograph of an RF-MEMS cantilevered series ohmic switch in CPW configuration. (b) Close-up of the micro-relay. The suspended cantilever is 180 μm long and 100 μm wide.

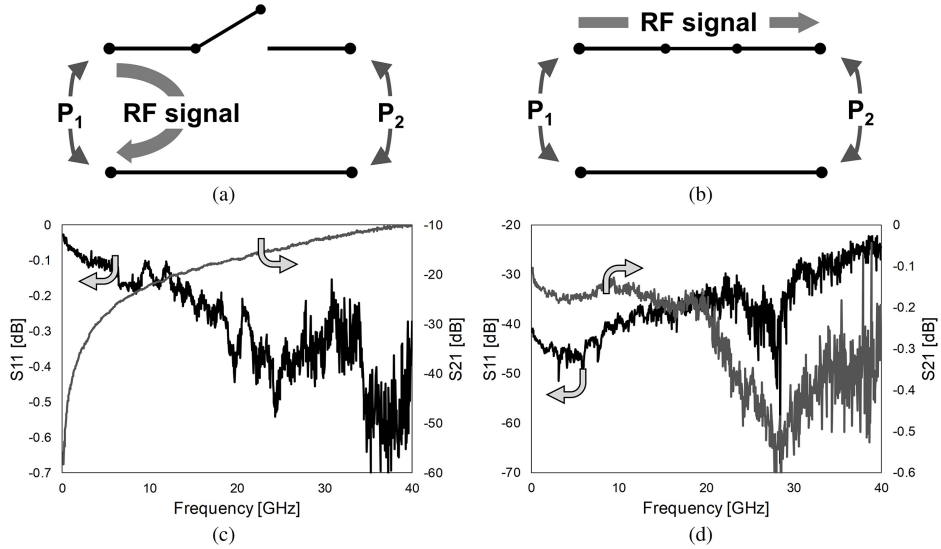

Figure 1.12. (a) Simplified schematic of the series ohmic micro-relay in figure 1.11 in the OPEN state (MEMS switch OFF). (b) Simplified schematic of the micro-relay in the CLOSED state (MEMS switch ON). (c) Measured reflection (S11) and isolation (S21) of the micro-relay in the OPEN state (MEMS switch OFF) from DC up to 40 GHz. (d) Measured reflection (S11) and transmission (S21) of the micro-relay in the CLOSED state (MEMS switch ON) from DC up to 40 GHz.

MEMS micro-relay is OFF, while figure 1.12(d) reports the reflection (S11) and transmission (S21) when the MEMS micro-relay is ON.

When OPEN, most of the power is reflected, as indicated by S11 in figure 1.12(c), which ranges between ~0 and −0.6 dB. Isolation (S21) is better than −25 dB up to 10 GHz, and better than −10 dB up to 40 GHz. The S21 worsens as the frequency

increases, because parasitic series capacitance is present between the suspended MEMS cantilever tip and the underlying contact area. When in the CLOSED state, the S11 is better than −25 dB up to 40 GHz, indicating a quite good impedance matching between the RF source and the MEMS device (see figure 1.12(d)). On the other hand, loss in transmission (S21) is very limited, being better than −0.5 dB up to 40 GHz. This result indicates the good quality of the ohmic contact between the pulled-in MEMS and the underlying metal area.

Figure 1.13 shows a microphotograph of an RF-MEMS shunt capacitive switch in a CPW configuration. In this case, the MEMS micro-relay is a membrane hinged at both ends (clamped–clamped configuration) to the ground planes, placed transversally across the RF line.

The behaviour of the shunt capacitive switch is dual with respect to the series ohmic one. First, no ohmic contact is established between the MEMS movable membrane and the RF underpass in any of the ON/OFF configurations, but, instead, a two-state capacitor. The capacitance realises a variable impedance path to the RF ground, rather than between the input and output terminations [62]. More details are reported in figure 1.14. When the MEMS is OFF, the distance between the floating capacitance plate and the underlying one is maximum, therefore the shunt capacitance is minimum (C_{min}), as shown in figure 1.14(a). Such a small capacitance realises a high-impedance path to ground that lets most parts of the RF signal travel between the input and output of the device (CLOSE switch). On the other hand, when the MEMS is ON (pulled-in), the shunt capacitance reaches the

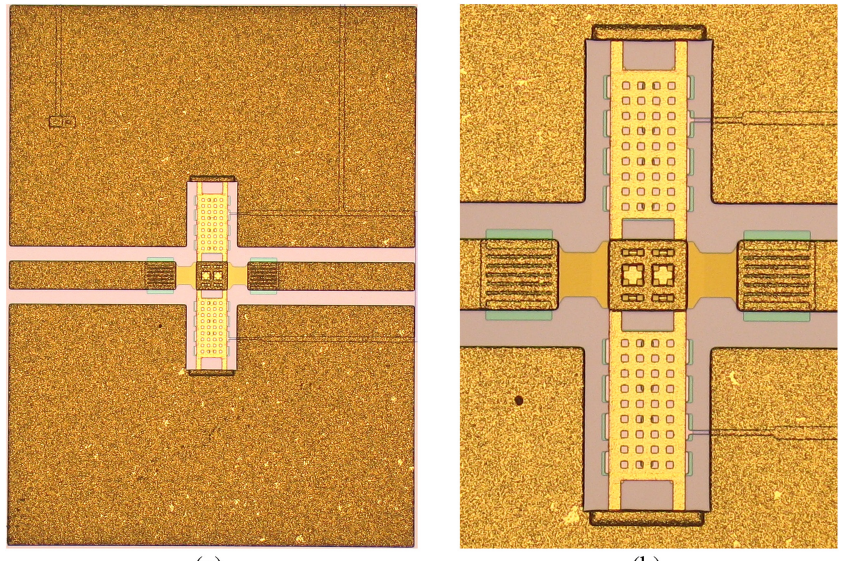

(a) (b)

Figure 1.13. (a) Microphotograph of an RF-MEMS clamped–clamped shunt capacitive switch in a CPW configuration. (b) Close-up of the micro-relay. The suspended double-hinged membrane is 180 μm long and 100 μm wide.

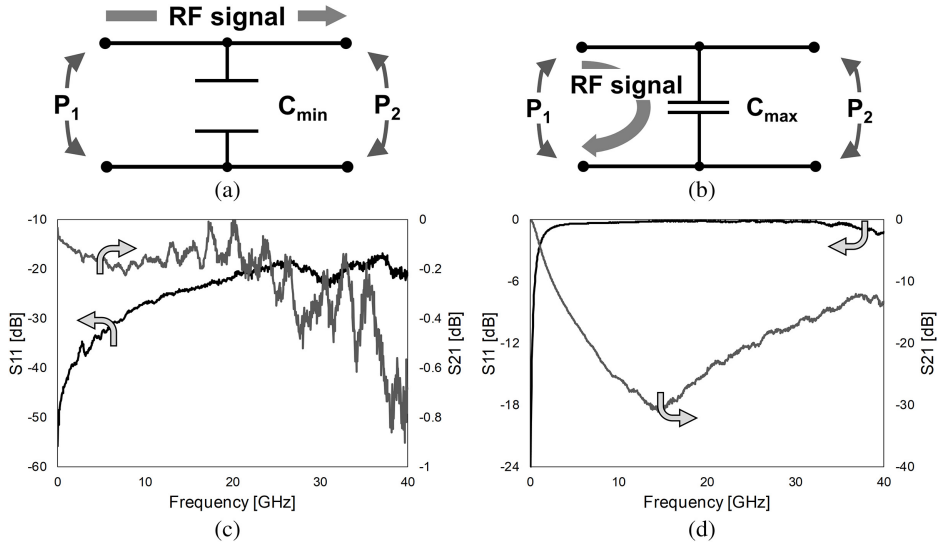

Figure 1.14. (a) Simplified schematic of the shunt capacitive micro-relay in figure 1.13 in the CLOSED state (MEMS switch OFF). (b) Simplified schematic of the micro-relay in the OPEN state (MEMS switch ON). (c) Measured reflection (S11) and transmission (S21) of the micro-relay in the CLOSED state (MEMS switch OFF) from DC up to 40 GHz. (d) Measured reflection (S11) and isolation (S21) of the micro-relay in the OPEN state (MEMS switch ON) from DC up to 40 GHz.

maximum value (C_{max}), as shown in figure 1.14(b). In this case, the large capacitance establishes a low-impedance path to ground that diverts most part of the RF signal travelling across the device, shorting it to ground (OPEN switch). The measured S-parameters of the shunt capacitive switch in figure 1.13 are reported in figure 1.14, referring to the range from DC up to 40 GHz.

In particular, the S-parameters for the MEMS in the OFF state (CLOSE switch) are reported in figure 1.14(c). Reflection (S11) is better than −20 dB up to 40 GHz, proving good impedance matching of the device. Moreover, loss in transmission (S21) is better than −0.8 dB up to 40 GHz. In contrast to the ohmic switch previously discussed, the S21 for the CLOSE switch exhibits increasing loss in the higher portion of the range. This is due to the shunt capacitance that, despite low (C_{min}), causes shorting to ground of a small part of the signal. In any case, having loss better than −1 dB up to 40 GHz is a very good performance result. Figure 1.14(d) shows the S-parameters for the MEMS in the ON state (OPEN switch). Starting from a few GHz, most part of the RF signal is reflected, as indicated by the S11 curve. On the other hand, isolation (S21) exhibits its best value, i.e. −30 dB, around 15 GHz. It is straightforward that capacitive switches, in contrast to ohmic micro-relays, are significantly influenced by the resonant behaviour of the reactive elements [61, 62]. Therefore, they cannot exhibit remarkable performance on a very wide band. Nonetheless, by exploiting their resonant characteristic, they can be optimised to outperform ohmic devices in very well defined frequency ranges.

As mentioned above, micro-relays are fundamental bricks enabling the pronounced reconfigurability of RF-MEMS technology. In light of this consideration, micro-switches have always been widely discussed in the literature, since the early days of RF-MEMS, with respect to various aspects of their design, topology, RF and electromechanical characteristics, reliability, power handling, and so on. For instance, the work reported in [63] discusses an RF-MEMS switching unit with pronounced long-term operability and cycling up to 1 billion in the K-band (18–27 GHz). Moreover, the switch concept discussed in [64] refers to an in-package commercial RF-MEMS device, suitable for 4G mobile applications. On the other hand, [65, 66] discuss novel realisations of RF-MEMS switches with improved performance. Concerning pull-in voltage reduction, designs exhibiting actuation levels as low as 5–7 V were demonstrated in the literature [67].

RF-MEMS variable capacitors (varactors)

From the conceptual point of view, an RF-MEMS variable capacitor (commonly referred to as varactor) is not significantly different from a capacitive switch. Therefore, when the variable capacitance is inserted in shunt-to-ground configuration, its behaviour is well described by the simplified circuit schematics previously shown in figure 1.14(a) and figure 1.14(b). Bearing in mind the discussion previously developed around the pull-in effect in electrostatically controlled MEMS, the varactor can be tuned in an analogue way (i.e. continuously) just from the rest position (zero bias) to the pull-in threshold, i.e. ranging across one-third of the overall air gap. After pull-in, the capacitance will abruptly commute to the maximum value.

The microphotograph in figure 1.15(a) shows an RF-MEMS varactor based on an electrostatically controlled floating gold electrode, kept suspended by four meander-shaped flexible beams.

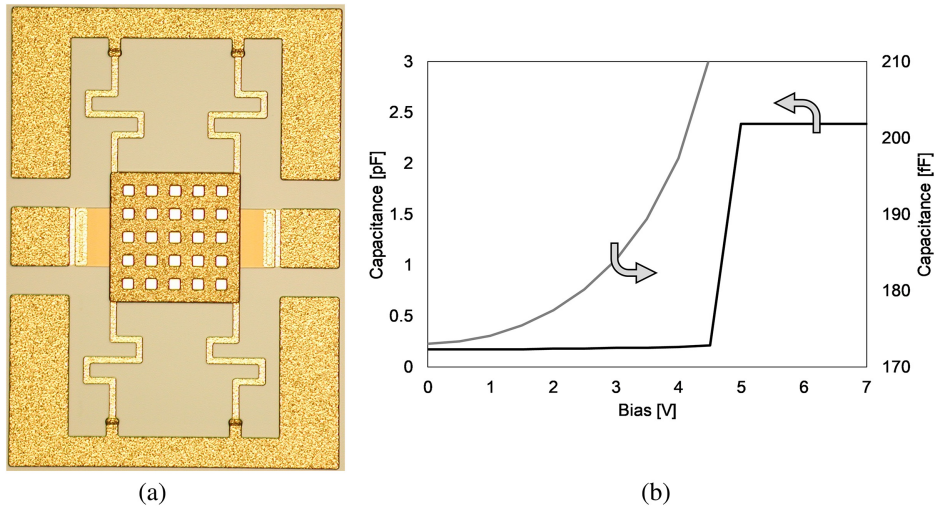

(a) (b)

Figure 1.15. (a) Microphotograph of an RF-MEMS clamped–clamped shunt variable capacitor (varactor) in a CPW configuration. (b) Measured capacitance versus bias voltage (C–V) characteristic. The capacitance can be controlled in an analogue fashion until the pull-in threshold is reached.

A fixed counter-electrode, lying beneath the movable MEMS, realises the second capacitor plate [67]. The plot reported in figure 1.15(b) shows the measured capacitance versus bias voltage (C–V) characteristic. Before pull-in, the capacitance ranges between ~170 fF and 210 fF (right vertical axis), and can be controlled continuously. When pulled-in, instead, the capacitance steps abruptly to ~2.4 pF (left vertical axis). Therefore, the ratio between the ON and OFF state capacitance (C_{on}/C_{off}) of the varactor in figure 1.15 is around 14, i.e. larger than one order of magnitude.

As for RF-MEMS switches, the scientific literature has always been populated by several contributions regarding varactors. To this purpose, an alternative design enabling a low-voltage controlled varactor is discussed in [68]. On the other hand, focusing on the extension of the varactor tuning range, the solution reported in [69] exploits the built-in intrinsic stress of the MEMS constitutive material, while [70] proposes a solution at the design level, featuring a double actuation mechanism. Again, concerning the linearity improvement in RF-MEMS varactors response, the work discussed in [71] exploits a double varactor with anti-bias control in order to improve such a characteristic. On the side of medium-/long-term reliability, a double DC biasing pulse is reported in [72] with the aim of decreasing the amount of charge entrapped in the insulating layer and, in turn, the so-called voltage screening (i.e. drifting of the pull-in/pull-out characteristic due to charge injection and dipoles orientation within the insulators).

RF-MEMS (variable) inductors

Given the discussion developed up to now, it is straightforward that RF-MEMS technology is also suitable for the realisation of high-performance inductors. The possibility to obtain suspended coils, as through a surface micromachining process featuring a sacrificial layer, as well as to manufacture metal lines above a thin substrate, as can be performed through etching the substrate from the back side (bulk micromachining), leads to a significant reduction of parasitic effects and, therefore, to an increase of the quality factor (Q-factor). The microphotograph in figure 1.16(a) depicts a suspended coil inductor in a CPW configuration. The plot in figure 1.16(b) shows the characteristic impedance of the inductor (S11) on a Smith chart, with reference to the frequency range from DC to 30 GHz.

The characteristic is always predominantly inductive, as confirmed by the trace mainly rotating in the upper half of the Smith chart. Another example of an air-suspended inductor, based on a different coil design, is reported in [73]. Despite the fact that the characteristic of tunability is not as critical for inductors as it is for capacitors, different approaches to tune inductance, triggered by the flexibility of RF-MEMS technology, have been reported in the literature. A fairly popular approach to enable the tunability of RF-MEMS inductors is the exploitation of suspended coils' non-planarity induced by the presence of residual stress within the patterned material. This leads to out-of-plane (i.e. vertical) displacement of adjacent coil turns, causing an inductance decrease if compared to the case of planarity. However, by driving a DC current through the coil, the heating induces a release of the intrinsic stress that temporarily improves the planarity and, therefore, increases the inductance value. Similarly, it is possible starting from a planar device in the rest

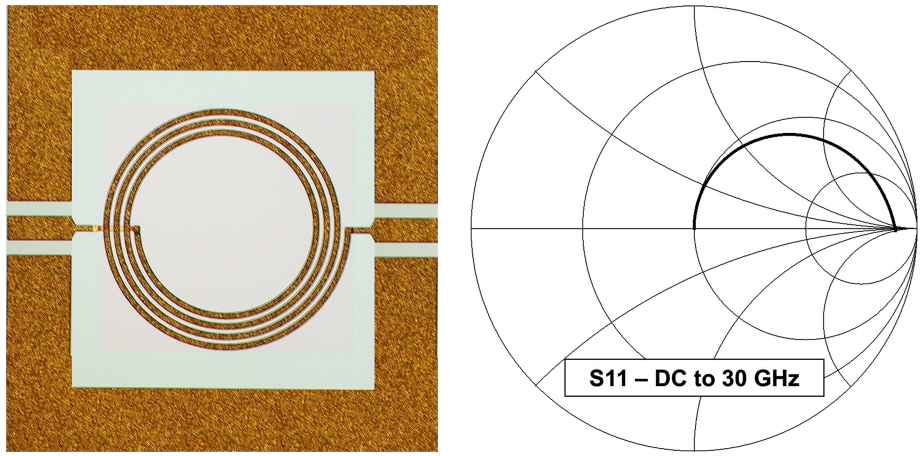

(a) (b)

Figure 1.16. (a) Microphotograph of an RF-MEMS suspended coil inductor in a CPW configuration. (b) Smith chart of the input characteristic impedance (S11) from DC to 30 GHz.

position to induce out-of-plane deformation by means of a bias current that reduces the inductance. Both these solutions are discussed in [74] and [75], respectively. A more exotic method to achieve inductor tunability is reported in [76]. In this case, a liquid is injected in the core, thus modifying its permeability and, therefore, the overall inductance value. More information and examples concerning high-performance (tunable) RF-MEMS inductors are developed in [77].

1.2.2 Complex reconfigurable passives in RF-MEMS technology

The discussion developed in the previous subsection outlined the most diffused classes of basic components realised in RF-MEMS technology. The common denominator of such groups is the implementation of a basic ON/OFF switching function (achievable in various ways), and/or of an actuation function that yields continuous (analogue) tunability within a certain range. Capitalising on the aforementioned basic components, and duplicating or combining them according to certain criteria within a unique physical device, it is possible to realise more complex RF-MEMS passive devices and networks, able to implement manipulation/treatment functions of RF/microwave/millimetre-wave signals, with highly pronounced tunability/reconfigurability. In the following sections, the most common classes of complex RF-MEMS networks will be reported.

RF-MEMS switching units and matrices

Starting from the most elemental RF-MEMS component, i.e. the micro-relay, its duplication and arrangement within a unique device enables the expansion of the switching function from an ON/OFF configuration between one input and output termination to multiple input and output branches. The microphotograph reported

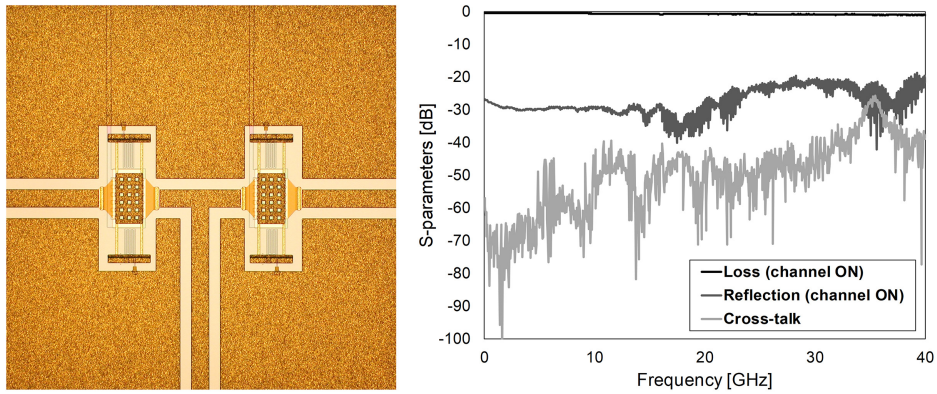

(a) (b)

Figure 1.17. (a) Microphotograph of an RF-MEMS Single Pole Double Throw (SPDT) in a CPW configuration. (b) Measured reflection, loss and isolation between adjacent channels (i.e. cross-talk), from DC to 40 GHz.

in figure 1.17(a) shows an RF-MEMS Single Pole Double Throw (SPDT) in a CPW configuration. In summary, it is a T-type switch with one input and two output terminations, each of the latter being controlled by an electrostatically driven RF-MEMS series ohmic switch. Depending on the ON/OFF configuration of the two (independently controllable) micro-relays, the input signal can be driven to each of the two outputs, to both or none of them.

The plot in figure 1.17(b) shows the measured S-parameter behaviour of the SPDT in the frequency range from DC to 40 GHz, and refers to a configuration in which one output channel is ON (CLOSE switch; pulled-in) while the other is OFF (OPEN switch; rest position). The transmission loss (S21) between the input and the conducting output branch is better than −1.1 dB and the reflection (S11) is better than −22 dB up to 40 GHz. Moreover, the isolation between the two output channels (S23), commonly addressed as cross-talk, ranges between −75 and −27 dB, and is always better than −45 dB up to 35 GHz.

The complexity of the switching unit can be increased, thus extending the order of the realised function. Starting from the configuration in figure 1.17, the number of output branches can be enlarged, leading, for instance, to Single Pole Four Throw (SP4T) switching units, in which there are four output terminations, as well as, more in general, to Single Pole Multiple Throw (SPMT) configurations. In addition, commutation can be performed across multiple inputs and outputs, leading to actual switching matrices (e.g. 2×2, 4×4, or $N \times N$) that can be effectively designed and manufactured in RF-MEMS technology. Several examples are reported in the literature, proving the achievement of remarkable characteristics, both for simpler switching units like SP4T [78–80], as well as for various order switching matrices [81–84].

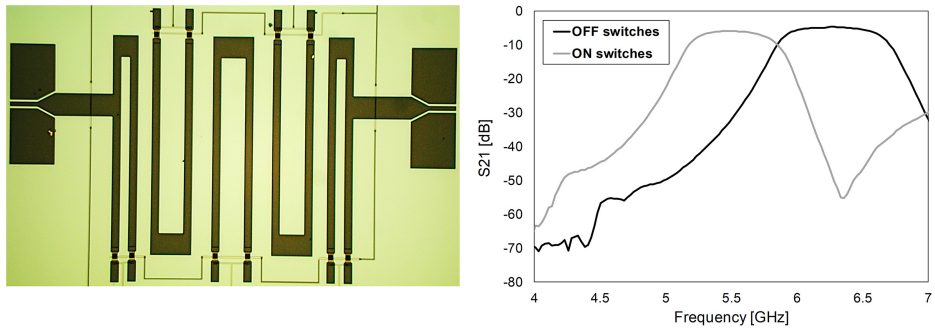

Figure 1.18. (a) Microphotograph of an RF-MEMS hairpin filter in a microstrip configuration. (b) Measured bandpass characteristic (S21) in two different network configurations.

RF-MEMS tunable filters

Following the same approach, i.e. adding switching functionalities, it is possible to enable tunability for other classes of passive devices, as in the case of RF filters. For instance, the hairpin filter configuration is well-known in the RF engineering community, and commonly exploited to shape a certain bandpass characteristic between the input and output terminations [85]. Such a class of filters was made tunable by implementing it in RF-MEMS technology, as discussed in [86] and depicted by the microphotograph in figure 1.18(a).

The hairpin filter exploits the inductive contribution of U-shaped bends and their capacitive coupling to shape the bandpass response. In the RF-MEMS hairpin filter (microstrip configuration) in figure 1.18, the length of each U-shaped element can be increased by adding a patch selected by cantilevered series ohmic switches, similar to the device previously reported in figure 1.11(a). Such a variation of geometry modifies the impedance of each U-shaped element, leading to a shift of the passed band. The measured transmission (S21) characteristic of the filter is shown in figure 1.18(b). When the MEMS switches are not actuated (short U-shaped elements), the passed band is centred around 6.3 GHz. On the other hand, when the MEMS micro-switches are pulled-in (long U-shaped elements), the passed band is centred around 5.5 GHz, i.e. about 1 GHz below.

The scientific literature is full of several significant contributions exploiting RF-MEMS devices to realise high-performance tunable/switchable RF filters. Differing from other classes of RF-MEMS complex networks, hybridisation/integration of MEMS with other technologies has been explored quite broadly. To this regard, several examples are reported concerning reconfigurable filters entirely realised in RF-MEMS technology [87–89]. Besides this option, different ways to obtain integrated RF-MEMS (commercially available) micro-switches with filters realised, for instance, in Printed Circuit Board (PCB) technology, were also investigated, in order to enable the desired tunability [90–93]. Furthermore, another technological solution of particular interest concerns the realisation of 3D (evanescent-mode) resonant cavities with a high Q-factor, which exploits RF-MEMS tunable elements (mainly varactors) to modify the filter bandpass characteristic [94–97].

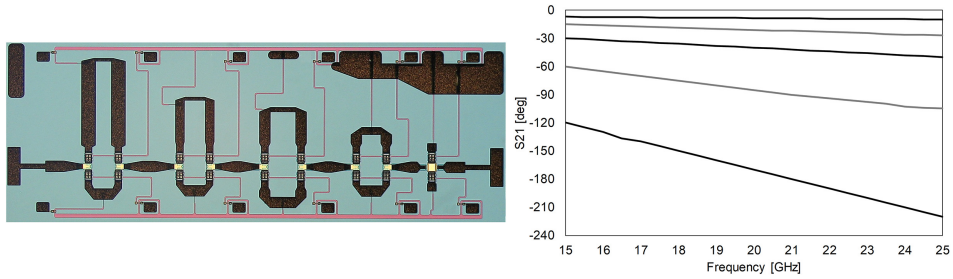

(a) (b)

Figure 1.19. (a) Microphotograph of an RF-MEMS 5-bit reconfigurable phase shifter in a microstrip configuration. (b) Input/output phase shift (S21) for different network configurations from 15 GHz to 25 GHz.

RF-MEMS reconfigurable phase shifters

Another class of passive devices that significantly benefits from the exploitation of RF-MEMS technology is that of reconfigurable phase shifters, particularly suited in the driving chain of electronically steerable antennas. An example of an RF-MEMS 5-bit reconfigurable phase shifter in a microstrip configuration is discussed in [98], and its microphotograph is shown in figure 1.19(a). The device features five switchable stages (i.e. 5-bit), in which two paths of different lengths can be selected (per each module) by means of RF-MEMS series ohmic switches. The longer denotes the path the RF signal has to travel across, and the larger denotes the phase shift of the output signal with respect to the input, observable through the S21 parameter. The reconfigurable phase shift of each stage (bit) is added to the others, as the five blocks are cascaded, thus leading to 32 possible configurations.

The plot reported in figure 1.19(b) shows the measured phase shift (S21) of the RF-MEMS network for a few different configurations, in the frequency range from 15 GHz to 25 GHz. Besides the previously discussed example, the scientific literature reports a wide variety of multi-state RF-MEMS phase shifters. In particular, relevant efforts were devoted to the development of multi-state digital devices [99–101], as well as of continually tunable networks [102, 103]. Also, interestingly, monolithic solutions in which the RF-MEMS phase shifter is designed and manufactured together with miniaturised reconfigurable antennas within the same technology platform have been reported [104–106].

RF-MEMS impedance-matching tuners

The availability of high-performance tunable reactive components, like varactors and inductors, as well as the ease of selection/deselection of fixed high Q-factor capacitances/inductances by means of low-loss ohmic switches, has also stimulated the exploitation of RF-MEMS technology for the realisation of impedance-matching tuners. An example of an impedance-matching network entirely realised in RF-MEMS technology is discussed in [107], and a microphotograph of a physical sample is reported in figure 1.20(a). The device, designed in a CPW configuration, features eight switching stages, based on cantilever-type RF-MEMS ohmic switches

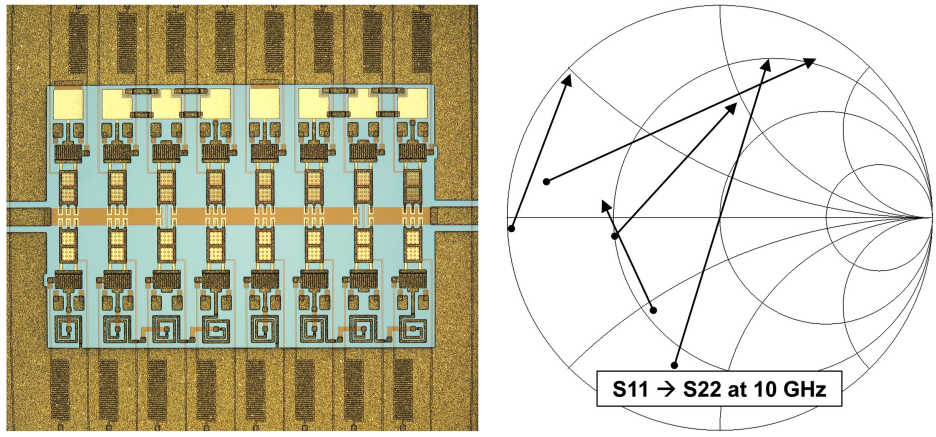

(a) (b)

Figure 1.20. (a) Microphotograph of an RF-MEMS 8-bit reconfigurable impedance-matching tuner in CPW configuration. (b) Smith chart showing the transformation operated by the device between the input (S11) and output (S22) characteristic impedance in a few configurations, at 10 GHz.

that, depending on their ON/OFF configuration, select different reactive components that load the RF line.

The RF-MEMS network is provided with two banks of reactive components, i.e. Metal-Insulator-Metal (MIM) capacitors, as visible in the upper part of figure 1.20(a), and in air-suspended inductors, as visible in the lower part of figure 1.20(a). These reactive elements are designed to be inserted both in series or a shunt configuration on the central RF line, depending on which switches are pulled-in and which are left in their rest position. In summary, the RF-MEMS network realises a double cascaded LC-ladder scheme [85], in which any series or shunt reactive element can be capacitive, inductive, both in parallel or neither selected, thus enabling 256 different impedance transformations. The Smith chart shown in figure 1.20(b) reports just a few among all functions performed by the impedance tuner. In the plot, each arrow shows how, per each configuration, the input characteristic impedance (S11) is transformed at the output (S22).

Despite not being densely populated, as is the case for other classes of devices, the scientific literature discusses several relevant examples of RF-MEMS impedance-matching tuners, proving quite extensive coverage of the Smith chart [108–111].

RF-MEMS programmable power attenuators

A category of complex networks that, despite being sporadically studied in the early years of RF-MEMS and recently attracting more attention in the research and industrial scientific community, is that of programmable (step) power attenuators for RF, microwave and millimetre-wave signals. One of the first examples discussed in the literature is reported in [112], while a microphotograph of the fabricated RF-MEMS network is shown in figure 1.21(a).

The RF-MEMS network features polycrystalline silicon buried resistors of different values, inserted along the RF line (series configuration). Moreover, cantilever-type

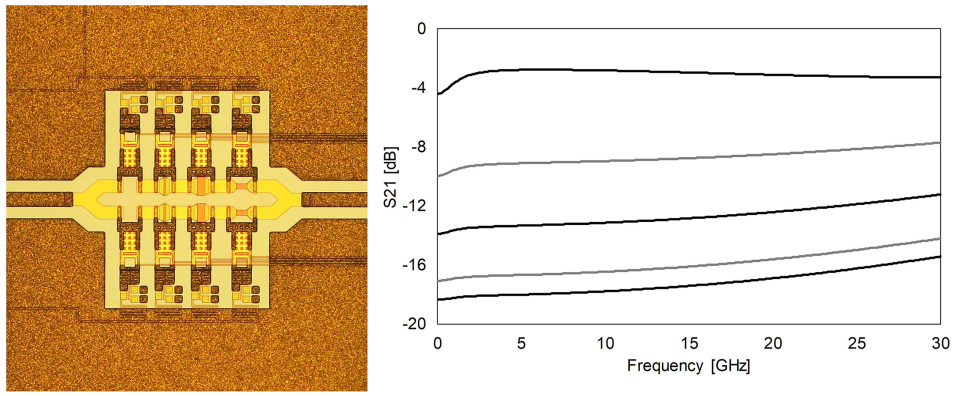

Figure 1.21. (a) Microphotograph of an RF-MEMS 4-bit programmable step attenuator in a CPW configuration. (b) Measured attenuation (S21) realised by the device in a few configurations, from DC to 30 GHz.

MEMS ohmic switches, with contact fingers before and after each loading resistor, are placed transversally along the device. When a MEMS switch is actuated (pulled-in), the fingers establish ohmic contact with the underneath metal pads, and a very-low-resistance path makes the RF signal flow through the gold switch membrane itself, rather than through the polycrystalline silicon buried resistor. In other words, the loading resistor is shorted, and therefore the attenuation implemented by the whole network is decreased. With particular reference to the device in figure 1.21(a), the whole attenuation can be stepped according to 4-bit, i.e. 16 different attenuation levels. The plot in figure 1.21(b) shows the measured attenuation (S21) in a few network configurations, ranging from DC to 30 GHz. Despite the fact that the characterised frequency range is rather wide, all the traces exhibit a quite flat characteristic and attenuation levels that can be set from around −3 to −20 dB.

Other implementations in RF-MEMS technology of multi-state step attenuators have been recently demonstrated in the literature, in some cases for measured frequency ranges as high as 110 GHz [113–115].

Miscellaneous RF-MEMS

In order to conclude this introductory chapter on RF-MEMS technology, other examples of basic components and complex networks, not covered by the previously reported classes, are going to be briefly listed.

The first category is of mechanical resonators based on MEMS technology. The reasons why they are not always classified as RF-MEMS are multiple. For one thing, often the frequency of operation is not in the RF/microwave/millimetre-wave range, but is lower. In addition, MEMS mechanical resonators are rarely tunable, and they are typically not framed in a waveguide configuration and do not feature switches or varactors. Beside these considerations purely related to a matter of definition, MEMS mechanical resonators are high-performance transducers exploiting a double conversion between physical domains, in order to operate a frequency

selection in a very narrow band. In more detail, a signal with a certain spectrum feeds the resonator, operating electrical to mechanical transduction. The MEMS device resonates at a certain mechanical frequency that is transduced back from a mechanical to electrical domain. The output electrical signal has a very narrow band with respect to the input one, and the frequency selection is operated by the mechanical characteristics of the MEMS resonator. Such a very selective filtering function is critical to devices like oscillators, which are meant to generate a reference (RF) frequency with pronounced stability versus time, and a bandwidth as narrow as possible around the carrier. MEMS mechanical resonators with a high Q-factor and remarkable stability against time and temperature have been widely reported in the literature [116–120]. The principle of the forth-and-back transduction between the electrical and mechanical domain is exploited also in other classes of frequency-filtering devices, like the so-called Surface Acoustic Wave (SAW) and Bulk Acoustic Wave (BAW) filters and (thin) Film Bulk Acoustic Resonators (FBARs). In this case, the input electrical signal (with a certain spectrum) is transduced into an acoustic wave that travels across a certain material, and then is transduced back into a narrowband electrical signal [121–124].

Another category of RF-MEMS devices is that of electromagnetic resonators and LC-tanks, necessary, for instance, to operate a precise selection of the RF frequency generated by Voltage Controlled Oscillators (VCOs). Differing from mechanical resonators, in this case there is no transduction from the electrical/electromagnetic to mechanical domain to operate selection of functionalities. The reactive (capacitive and inductive) characteristics of the device determine its specific resonance that, therefore, shapes the output signal. Electromagnetic resonators and LC-tanks significantly benefit from the intrinsic reconfigurability of RF-MEMS, extensively discussed above. For example, it is sufficient to realise part of the capacitive contribution of LC-tanks by means of an RF-MEMS varactor, in order to enable wide tunability of the filtering function operated by the whole device. The scientific literature describes various implementations of electromagnetic resonators and LC-tanks in RF-MEMS technology, both concerning design concepts in planar technology [125, 126], as well as exploiting 3D (evanescent-mode) resonant cavities featuring tunable elements [127, 128].

Other RF-MEMS devices of interest in modern RF components and systems are directional couplers/splitters. These passives are meant to couple different signals in order to perform certain mixing functionalities, e.g. of critical importance in RF transmitters/receivers (transceivers), as well as in Automated Test Equipment (ATE) systems, like Vector Network Analysers (VNAs). As it is easy to envisage, the intrinsic tunability of RF-MEMS enables pronounced reconfigurability of couplers/splitters, both concerning selection of different RF signals to be mixed together, as well as with reference to the extent (in terms of dB) according to which such signals must be coupled or split. As for other categories of RF-MEMS, the scientific literature on directional couplers/splitters is populated by several significant contributions, discussing various design concepts and diverse solutions in terms of micro-fabrication technology platforms [129–135].

Returning to programmable phase shifters, a sub-class of RF-MEMS devices is the so-called True-Time Delay Lines (TTDLs). These reconfigurable networks are,

in fact, phase shifters with a quite pronounced linearity of the phase shift over frequency. This characteristic ensures True-Time Delay (TTD), which is a constant (i.e. invariant) delay with respect to frequency. Relevant papers discuss TTDLs in RF-MEMS technology, as well as the achieved remarkable characteristics in terms of reconfigurability [136–140].

Finally, to conclude this chapter, the flexibility of RF-MEMS technology in implementing treatment functionalities of RF/microwave/millimetre-wave signals has unequivocally emerged, in enabling high-performance, pronounced reconfigurability/tunability and wideband operation over frequency. In the following approaches, similar to those discussed in the previous sections, RF designers and engineers now have the possibility to conceive innovative design concepts dedicated to the implementation of RF-MEMS passives with characteristics that transcend those reported up to now. Additionally, blending more functionalities, such as, for example, reconfigurable phase shifting with multi-level step attenuation, within the same RF-MEMS physical device, is also a viable option holding a not-so-hidden potential, especially bearing in mind emerging 5G as well as beyond-5G applications.

1.3 Conclusion

This chapter developed a general discussion on Micro-ElectroMechanical Systems (MEMS) and MEMS for Radio Frequency passives (RF-MEMS) technologies. First, the inception of the concept of microsystems was analysed with reference to the evolution of semiconductor technologies, highlighting common features as well as how they can be differentiated. To this regard, a brief discussion was developed around the evolution of (standard) semiconductor technologies, also including the driving trend of Moore's law, which basically described, and still continues to describe, decades of transistors' technology evolution. It was also remarked that, in parallel to the maturation and consolidation of standard semiconductor technologies, experimentation of micro-fabrication steps devoted to obtaining microsystems, i.e. micro-devices with mechanical properties, began in the late 1960s. Then, the first examples of actual MEMS devices, reported in the literature in the second half of the 1970s, were also discussed.

The most widely exploited technology process flows for the realisation of MEMS, namely surface and bulk micromachining, were also described, focusing on their fundamental characteristics and on the typical features distinguishing one from the other. Still referring to the intricate relationship between MEMS and standard semiconductor technologies, the concepts of '*More Moore*' and of '*More than Moore*' were debated, putting under the spotlight the opposite trends that microsystems and semiconductors follow concerning miniaturisation and customisation.

The concept of RF-MEMS was then introduced, stressing the relative novelty of this kind of microsystem exploitation as compared to sensors and actuators, such as, for example, inertial sensors (accelerometers and gyroscopes) and micro-mirrors.

The four main driving mechanisms to control RF-MEMS devices (electrostatic, electromagnetic, piezoelectric, thermoelectric) were reviewed. Fundamental physical considerations were also included regarding electrostatic actuation of RF-MEMS, it

being one of the most diffused, as well as that exploited in the practical examples that will be listed throughout this book.

Subsequently, the most common categories of RF-MEMS devices were introduced, focusing both on simple components as well as on complex high-order reconfigurable networks. Concerning the former, micro-relays (or switches), variable capacitors (varactors) and inductors were reported. With reference to the latter, instead, several classes of complex RF-MEMS networks were discussed, among which are complex switching units, programmable step attenuators, impedance-matching tuners, and so on. For all of the aforementioned categories of RF-MEMS, typical design implementations and experimentally observed performance/characteristics have been shown.

References

[1] Brock D C and Moore G E 2006 *Understanding Moore's Law: Four Decades of Innovation* 1st edn (Philadelphia, PA: Chemical Heritage Foundation) p 122

[2] *Converter Passion ADC Performance Evolution: Low-Voltage Operation—Part 2* https://converterpassion.wordpress.com/tag/cmos/)

[3] Zhang G Q and van Roosmalen A 2009 *More than Moore—Creating High Value Micro/Nanoelectronics Systems* 1st edn (Berlin: Springer) p 332

[4] Hobstetter J H 1960 Mechanical properties of semiconductors *Properties of Crystalline Solids* 1st edn (West Conshohocken, PA: ASTM) p 40

[5] Beams J W, Freazeale J B and Bart W L 1955 Mechanical strength of thin films of metals *Phys. Rev. Lett.* **100** 1657–61

[6] Neugebauer C A 1960 Tensile properties of thin, evaporated gold films *J. Appl. Phys.* **31** 1096–101

[7] Blakely J M 1964 Mechanical properties of vacuum-deposited gold *J. Appl. Phys.* **35** 1756–9

[8] Bassous E 1978 Fabrication of novel three-dimensional microstructures by the anisotropic etching of (100) and (110) silicon *IEEE Trans. Electron. Dev.* **25** 1178–85

[9] Wen H K, Hynecek J and Boettcher S F 1979 Development of a miniature pressure transducer for biomedical applications *IEEE Trans. Electron. Dev.* **26** 1896–905

[10] Roylance L M and Angell B J 1979 A batch-fabricated silicon accelerometer *IEEE Trans. Electron. Dev.* **26** 1911–17

[11] Chen P, Muller R, Shiosaki T and White R 1979 WP-B6 silicon cantilever beam accelerometer utilizing a PI-FET capacitive transducer *IEEE Trans. Electron. Dev.* **26** 1857

[12] Petersen K E 1979 Micromechanical membrane switches on silicon *IBM J. Res. Dev.* **23** 376–85

[13] Petersen K E 1977 Micromechanical light modulator array fabricated on silicon *Appl. Phys. Lett.* **31** 521

[14] Petersen K E 1982 Silicon as a mechanical material *Proc. IEEE* **70** 420–57

[15] Bustillo J, Howe R and Muller R 1998 Surface micromachining for microelectromechanical systems *Proc. IEEE* **86** 1552–74

[16] Howe R T and Muller R S 1983 Polycrystalline silicon micromechanical beams *J. Electrochem. Soc.* **130** 1420–23

[17] Howe R and Muller R 1986 Resonant-microbridge vapor sensor *IEEE Trans. Electron. Dev.* **33** 499–506

[18] Fan L S, Tai Y C and Muller R S 1987 *Pin Joints, Gears, Springs, Cranks, and Other Novel Micromechanical Structures* (Oak Ridge, TN: OSTI) https://osti.gov/scitech/biblio/5974687
[19] Fan L S, Tai Y C and Muller R S 1989 IC-processed electrostatic micromotors *Sensors Actuators* **20** 41–7
[20] Jaeger R C 1988 *Introduction to Microelectronic Fabrication* 1st edn (Boston, MA: Addison-Wesley) p 232
[21] Gualtieri D Interdisciplinarity in Physics *Tikalon Blog* http://tikalon.com/blog/blog.php?article=2012/interdiscipline)
[22] Li H, Li D, Hu Y, Pan P, Li T and Feng J 2016 UV-LIGA microfabrication for high frequency structures of a 220GHz TWT amplifier *Proc. IEEE Int. Vacuum Electron. Conf. (IVEC) (Monterey, CA, April)* pp 131–3
[23] Rusch C, Börner M, Mohr J, Zwick T, Chen Y and De Los Santos H J 2013 Electrical tuning of dielectric resonators with LIGA-MEMS *Proc. Europ. Microw. Integrated Circ. Conf. (Nuremberg, Oct. 2013)* pp 316–9
[24] Johnstone R W and Parmaswaran A 2004 *An Introduction to Surface-Micromachining* 1st edn (Berlin Springer) p 189
[25] Franssila S 2010 *Introduction to Microfabrication* 2nd edn (New York: Wiley) p 534
[26] Iannacci J, Tschoban C, Reyes J, Maaß U, Huhn M, Ndip I and Pötter H 2016 RF-MEMS for 5G mobile communications: a basic attenuator module demonstrated up to 50 GHz *Proc. IEEE SENSORS (Orlando, FL, Oct.–Nov. 2016)* pp 131–3
[27] Pal P and Sato K 2017 *Silicon Wet Bulk Micromachining for MEMS* 1st edn (Boca Raton, FL: CRC Press) p 424
[28] Tilli M, Motooka T, Airaksinen V-M, Franssila S, Paulasto-Krockel M and Lindroos V 2015 *Handbook of Silicon Based MEMS Materials and Technologies* 2nd edn (Norwich, NY: William Andrew) p 826
[29] Iannacci J, Sordo G, Serra E and Schmid U 2016 The MEMS four-leaf clover wideband vibration energy harvesting device: design concept and experimental verification *Microsyst. Technol.* **22** 1865–81
[30] Sherman S J, Tsang W K, Core T A and Quinn D E 1992 *A low cost monolithic accelerometer Proc. of VLSI Circ. Symp. (Seattle, WA, June 1992)* pp 34–5
[31] Iannacci J 2015 Reliability of MEMS: a perspective on failure mechanisms, improvement solutions and best practices at development level *Displays* **37** 62–71
[32] Sensors Online *The Growing Presence of MEMS and MST in Automotive Applications* https://dialnet.unirioja.es/servlet/articulo?codigo=486778
[33] National Inventors Hall of Fame *Larry Hornbeck, Digital Micromirror Device* https://invent.org/inductees/larry-hornbeck
[34] Douglass M R 1998 Lifetime estimates and unique failure mechanisms of the Digital Micromirror Device (DMD) *Proc. of IEEE Int. Reliab. Phys. Symp. (Reno, NV, April 1998)* p 9–16
[35] *Growth, Trends, COVID-19 Impact, and Forecasts* https://mordorintelligence.com/industry-reports/global-mems-based-inertial-measurement-unit-market
[36] Econocom *How the Internet of Things Is Revolutionising Industry* https://blog.econocom.com/en/blog/how-the-internet-of-things-is-revolutionising-industry/
[37] McGrath W R, Walker C, Yap M and Tai Y C 1993 Silicon micromachined waveguides for millimeter-wave and submillimeter-wave frequencies *IEEE Microw. Guid. Wave Lett* **3** 61–3

[38] Katehi L P B, Rebeiz G M, Weller T M, Drayton R F, Cheng H J and Whitaker J F 1993 Micromachined circuits for millimeter- and sub-millimeter-wave applications *IEEE Antennas Propag. Mag.* **35** 9–17
[39] Weller T M and Katehi L P B 1995 Compact stubs for micromachined coplanar waveguide *Proc. 25th Europ. Microw. Conf. (Bologna, Sept. 1995)* pp 589–93
[40] Mahmoud S F 1991 *Electromagnetic Waveguides: Theory and Applications* 1st edn (London: Peter Peregrinus) p 240
[41] Iannacci J 2013 RF passive components for wireless applications *Handbook of MEMS for Wireless and Mobile Applications* 1st edn (Cambridge: Woodhead Publishing) pp 100–35
[42] Pozar D M 2005 *Microwave Engineering* 2nd edn (New York: Wiley) p 716
[43] Wadell B 1991 *Transmission Line Design Handbook* 1st edn (Norwood, MA: Artech House)
[44] Yang S, Hu Z, Buchanan N B, Fusco V F, Stewart J A C, Wu Y, Armstrong B M, Armstrong G A and Gamble H S 1998 Characteristics of trenched coplanar waveguide for high-resistivity Si MMIC applications *IEEE Trans. Microw. Theory Tech* **46** 623–31
[45] Farrington N E S and Iezekiel S 2011 Design and simulation of membrane supported transmission lines for interconnects in a MM-wave multichip module *Prog. Electromag. Res. B* **27** 165–86
[46] Shi Y, Lai Z, Xin P, Shao L and Zhu Z 2001 Design and fabrication of micromachined microwave transmission lines *Proc. SPIE* **4557** 477–84
[47] Goldsmith C L, Yao Zhimin Eshelman S and Denniston D 1998 Performance of low-loss RF MEMS capacitive switches *IEEE Microw. Guid. Wave Lett.* **8** 269–71
[48] Feng Z, Zhang W, Su B, Harsh K F, Gupta K C, Bright V and Lee Y C 1999 Design and modeling of RF MEMS tunable capacitors using electro-thermal actuators *Proc. IEEE MTT-S Int. Microw. Symp. (Anaheim, CA, June 1999)* pp 1507–10
[49] Katehi L P B, Rebeiz G M and Nguyen C T- 1998 MEMS and Si-micromachined components for low-power, high-frequency communications systems *Proc. IEEE MTT-S Int. Microw. Symp. (Baltimore, MD, June 1998)* pp 331–3
[50] Malczewski A, Eshelman S, Pillans B, Ehmke J and Goldsmith C L 1999 X-band RF MEMS phase shifters for phased array applications *IEEE Microw. Guid. Wave Lett.* **9** 517–9
[51] Liu C 2011 *Foundations of MEMS* 2nd edn (London: Pearson Education) p 560
[52] Lee H S, Leung C H, Shi J and Chan S C 2004 Micro-electro-mechanical relays-design concepts and process demonstrations *Proc. 50th IEEE Holm Conf. on Electrical Contacts and the 22nd Int. Conf. on Electrical Contacts (Seattle, WA, Sept. 2004)* pp 242–7
[53] Cho I-J, Song T, Baek S-H and Yoon E 2005 A low-voltage and low-power RF MEMS series and shunt switches actuated by combination of electromagnetic and electrostatic forces *IEEE Trans. Microw. Theory Tech* **53** 2450–7
[54] Safari A and Akdoğan E K 2008 *Piezoelectric and Acoustic Materials for Transducer Applications* 1st edn (New York: Springer) p 482
[55] Kawakubo T, Nagano T, Nishigaki M, Abe K and Itaya K 2005 Piezoelectric RF MEMS tunable capacitor with 3V operation using CMOS compatible materials and process *Proc. IEEE Int. Electron Dev. Meet. IEDM (Washington, DC, Dec. 2005)* pp 294–7
[56] Daneshmand M, Fouladi S, Mansour R R, Lisi M and Stajcer T 2009 Thermally-actuated latching RF MEMS switch *Proc. IEEE Int. Microw. Symp. MTT-S Digest (Boston, MA, June 2009)* pp 1217–20

[57] Iannacci J, Faes A, Repchankova A, Tazzoli A and Meneghesso G 2011 An active heat-based restoring mechanism for improving the reliability of RF-MEMS switches *Microelectron. Reliab.* **51** 1869–73
[58] Iannacci J, Repchankova A, Faes A, Tazzoli A, Meneghesso G and Dalla Betta G F 2010 Enhancement of RF-MEMS switch reliability through an active anti-stiction heat-based mechanism *Microelectron. Reliab.* **50** 1599–603
[59] Senturia S D 2001 *Microsystem Design* 1st edn (New York: Springer) p 689
[60] Giacomozzi F, Mulloni V, Colpo S, Iannacci J and Margesin B 2011 Faes A flexible fabri-cation process for RF MEMS devices Rom. *J. Inf. Sci. Technol. (ROMJIST)* **14** 259–68
[61] Iannacci J, Resta G, Farinelli P and Sorrentino R 2012 RF-MEMS components and networks for high-performance reconfigurable telecommunication and wireless systems *Trans. Tech. Pub. Adv. Sci. Tech* **81** 65–74
[62] Iannacci J 2013 *Practical* Guide *to RF-MEMS* 1st edn (Weinheim: Wiley-VCH) p 372
[63] Carty E, Fitzgerald P, McDaid P, Stenson B and Goggin R 2016 Development of a DC to K-band ultra long on-life RF MEMS switch with integrated driver circuitry *Proc. 11th Europ. Microw, Integrated Circ. Conf. EuMIC (London, Oct. 2016)* pp 444–7
[64] Seki T, Yamamoto J, Murakami A, Yoshitake N, Hinuma K-i Fujiwara T, Sano K, Matsushita T, Sato F and Oba M 2013 An RF MEMS switch for 4G Front-Ends *Proc. IEEE MTT-S Int. Microw. Symp. IMS (Seattle, WA, June 2013)* pp 131–3
[65] Chu C, Liao X and Yan H 2017 Ka-band RF MEMS capacitive switch with low loss, high isolation, long-term reliability and high power handling based on GaAs MMIC technology *IET Microw. Antennas Propag.* **11** 942–8
[66] Ma L Y, Soin N and Nordin A N 2016 *A novel design of low-voltage low-loss K-band RF-MEMS capacitive switch Proc. Symp. on Design, Test, Integr. and Packaging of MEMS/MOEMS DTIP (Budapest, May–June 2016)* pp 151–5
[67] Iannacci J, Gaddi R and Gnudi A 2007 *Non-linear electromechanical RF model of a MEMS varactor based on veriloga© and lumped-element parasitic network Proc. Europ. Microw. Integ. Circ. Conf. (Munich, Oct. 2007)* pp 544–7
[68] Elshurafa A M, Ho P H and Salama K N 2012 Low voltage RF MEMS variable capacitor with linear C–V response *IET Electron. Lett.* **48** 392–3
[69] Nishiyama M, Konishi H, Suzuki J, Tezuka Y, Suzuki Y and Suzuki K 2007 *Extremely high capacitance ratio (C/R) RF MEMS variable capacitor with chameleon actuators Proc. Int. Solid-State Sensors, Actuators and Microsyst. Conf. TRANSDUCERS (Lyon, June 2007)* pp 631–4
[70] Cazzorla A, Sorrentino R and Farinelli P 2015 *Double-actuation extended tuning range RF MEMS Varactor Proc. Europ. Microw. Conf. EuMC (Paris, Oct. 2015)* pp 937–40
[71] Chen K, Kovacs A and Peroulis D 2010 *Anti-biased RF MEMS varactor topology for 20–25 dB linearity enhancement Proc. IEEE MTT-S Int. Microw. Symp. (Anaheim, CA, May 2010)* pp 1142–5
[72] Ikehashi T *et al* 2008 *An RF MEMS variable capacitor with intelligent bipolar actuation Proc. IEEE Int. Solid-State Circ. Conf. (San Francisco, CA, Feb. 2008)* pp 582–637
[73] Mizuochi Y, Amakawa S, Ishihara N and Masu K 2009 *Study of air-suspended RF MEMS inductor configurations for realizing large inductance variations Proc. Argentine School of Micro-Nanoelectronics, Tech. and Applications (San Carlos de Bariloche, Oct. 2009)* pp 550–5

[74] Chang S and Sivoththaman S 2006 A tunable RF MEMS inductor on silicon incorporating an amorphous silicon bimorph in a low-temperature process *IEEE Electron Dev. Lett.* **27** 905–7

[75] Zine-El-Abidine I, Okoniewski M and McRory J G 2004 *A tunable RF MEMS inductor Proc. Int. Conf. on MEMS, NANO and Smart Syst. ICMENS (Banff, Aug 2004)* pp 636–8

[76] Banitorfian F, Eshghabadi F, Manaf A A, Pons P, Noh N M, Mustaffa M T and Sidek O 2013 *A novel tunable water-based RF MEMS solenoid inductor Proc. IEEE Regional Symp. on Micro and Nanoelectron. RSM (Langkawi, Sept. 2013)* pp 58–61

[77] Hikmat O F and Mohamed Ali M S 2017 RF MEMS inductors and their applications—a review *IEEE J. Microelectromech. Syst.* **26** 17–44

[78] Casini F, Farinelli P, Mannocchi G, DiNardo S, Margesin B, De Angelis G, Marcelli R, Vendier O and Vietzorreck L 2010 *High performance RF-MEMS SP4T switches in CPW technology for space applications Proc. Europ. Microw. Conf. (Paris, Sept. 2010)* pp 89–92

[79] Yang H-H, Yahiaoui A, Zareie H, Blondy P and Rebeiz G M 2014 *A compact high-isolation DC-50 GHz SP4T RF MEMS switch Proc. IEEE MTT-S Int. Microw. Symp. IMS (Tampa, FL, June 2014)* pp 141–4

[80] Zareie H and Rebeiz G M 2014 Compact high-power SPST and SP4T RF MEMS metal-contact switches *IEEE Trans. Microw. Theory Tech.* **62** 297–305

[81] Chan K Y, Ramer R and Mansour R R 2012 Novel miniaturized RF MEMS staircase switch matrix *IEEE Microw. Wirel. Comp. Lett.* **22** 117–19

[82] Daneshmand M and Mansour R R 2011 RF MEMS satellite switch matrices *IEEE Microw. Mag.* **12** 92–109

[83] Fomani A A and Mansour R R 2009 Monolithically integrated multiport RF MEMS switch matrices *IEEE Trans. Microw. Theory Tech.* **57** 3434–41

[84] Fomani A A and Mansour R R 2009 *Miniature RF MEMS switch matrices Proc. IEEE MTT-S Int. Microw. Symp. IMS (Boston, MA, June 2009)* pp 1221–4

[85] Besser L and Gilmore R 2003 *Practical RF Circuit Design for Modern Wireless Systems: Passive circuits and systems* 1st edn (Norwood, MA: Artech House) p 576

[86] Ocera A, Farinelli P, Mezzanotte P, Sorrentino R, Margesin B and Giacomozzi F 2006 *A novel MEMS-tunable hairpin line filter on silicon substrate Proc. Europ. Microw. Conf. (Manchester, Sept. 2006)* pp 803–6

[87] Reines I, Park S J and Rebeiz G M 2010 Compact low-loss tunable X-band bandstop filter with miniature RF-MEMS switches *IEEE Trans. Microw. Theory Tech.* **58** 1887–95

[88] Hsu H H, Margomenos A D and Peroulis D 2011 *A monolithic RF-MEMS filter with continuously-tunable center-frequency and bandwidth Proc. IEEE Top. Meet. on Silicon Monolithic Integr. Circ. in RF Syst. (Phoenix, AZ, Jan. 2011)* pp 169–72

[89] Shah U, Sterner M and Oberhammer J 2011 *Basic concepts of moving-sidewall tuneable capacitors for RF MEMS reconfigurable filters Proc. Europ. Microw. Integ. Circ. Conf. (Manchester, Oct. 2011)* pp 526–9

[90] Shojaei-Asanjan D and Mansour R R 2017 The sky's the limit: A switchable RF-MEMS filter design for wireless avionics intracommunication *IEEE Microw. Mag.* **18** 100–6

[91] Wang H, Anand A and Liu X 2017 *A miniature 800–1100-MHz tunable filter with high-Q ceramic coaxial resonators and commercial RF-MEMS tunable digital capacitors Proc.*

IEEE Wireless and Microw. Tech. Conf. WAMICON (Cocoa Beach, FL, April 2017) pp 131–3

[92] Kumar N and Singh Y K 2017 RF-MEMS-based bandpass-to-bandstop switchable single- and dual-band filters with variable FBW and reconfigurable selectivity *IEEE Trans. Microw. Theory Tech.* pp 1–14

[93] Hickle M D, Li J, Psychogiou D and Peroulis D 2016 A high-performance pathway: a 0.95/2.45-GHZ switched-frequency bandpass filter using commercially available RF MEMS tuning elements *IEEE Microw. Mag.* **17** 34–41

[94] Stefanini R, Chatras M, Pothier A, Guines C and Blondy P 2013 *High-Q 3D tunable RF MEMS filter with a constant fractional bandwidth Proc. Europ. Microw. Integr. Circ. Conf. (Nuremberg, Oct. 2013)* pp 312–5

[95] Chan K Y, Ramer R and Mansour R R 2017 A switchable iris bandpass filter using RF MEMS switchable planar resonators *IEEE Microw. Wirel. Comp. Lett.* **27** 34–6

[96] Park S J, Reines I, Patel C and Rebeiz G M 2010 High-Q RF-MEMS 4–6-GHz tunable evanescent-mode cavity filter *IEEE Trans. Microw. Theory Tech.* **58** 381–9

[97] Schulte B, Ziegler V, Schoenlinner B, Prechtel U and Schumacher H 2011 *RF-MEMS tunable evanescent mode cavity filter in LTCC technology at Ku-band Proc. of Europ. Microw. Integr. Circ. Conf. (Manchester, Oct. 2011)* pp 514–7

[98] Bastioli S, Di Maggio F, Farinelli P, Giacomozzi F, Margesin B, Ocera A, Pomona I, Russo M and Sorrentino R 2008 *Design manufacturing and packaging of a 5-bit K-band MEMS phase shifter Proc. Europ. Microw. Integr. Circ. Conf. (Amsterdam, Oct. 2008)* pp 338–41

[99] Ramli N A and Arslan T 2017 *Design and simulation of a 2-bit distributed S-band MEMS phase shifter Proc. Int. Conf. Thermal, Mech. and Multi-Physics Simul. and Exp. in Microelectron.and Microsyst. EuroSimE (Dresden, April 2017)* pp 1–5

[100] Dey S and Koul S K, *2014 10 –35-GHz frequency reconfigurable RF MEMS 5-bit DMTL phase shifter uses push-pull actuation based toggle mechanism Proc. IEEE Int. Microw. and RF Conf. IMaRC (Bangalore, Dec. 2014)* pp 21–4

[101] Bakri-Kassem M, Mansour R R and Safavi-Naeini S 2014 *A novel latching RF MEMS phase shifter Proc. Europ. Microw. Integr. Circ. Conf. (Rome, Oct. 2014)* pp 668–71

[102] McFeetors G and Okoniewski M 2004 *Analog tunable microwave phase shifters using RF MEMS Proc. Int. Symp. on Antenna Tech. and Appl. Electromagnetics and URSI Conf. (Ottawa, July 2004)* pp 141–4

[103] Unlu M, Demir S and Akin T 2013 A 15–40-GHz frequency reconfigurable RF MEMS phase shifter IEEE Trans. Microw. *Theory Tech.* **61** 2865–77

[104] Abumunshar A J, Nahar N K, Hyman D and Sertel K 2017 18 *–40GHz low-profile phased array with integrated MEMS phase shifters Proc. Europ. Conf. on Antennas and Propagation EUCAP (Paris, March 2017)* pp 2800–1

[105] Yeo W G, Nahar N K and Sertel K 2013 *Phased array antenna with integrated MEMS phase shifters for Ka-band SATCOM Proc. IEEE Antennas and Propagation Soc. Int. Symp. APSURSI (Orlando, FL, July 2013)* pp 105–6

[106] Das A, Puri M and Sengar J S 2013 *A novel monolithic integrated phased array antenna using 4-bit distributed MEMS phase shifter and triangular patch antenna Proc. Int. Conf. on Adv. in Comput., Commun. and Informatics ICACCI (Mysore, Aug. 2013)* pp 913–8

[107] Iannacci J, Masotti D, Kuenzig T and Niessner M 2011 *A reconfigurable impedance matching network entirely manufactured in RF-MEMS technology* Proc. (SPIE) **8066** 280–91

[108] Festo A E, Folgero K, Ullaland K and Gjertsen K M 2009 A six bit, 6–18 GHz *RF-MEMS impedance tuner for 50 Ω systems Proc. Europ. Microw. Conf. EuMC (Rome, Sept.–Oct. 2009)* pp 1132–5

[109] Vaha-HeikkiIa T, Varis J, Tuovinen J and Rebeiz G M 2004 *A V-band single-stub RF MEMS impedance tuner Proc. Europ. Microw. Conf. (Amsterdam, Oct. 2004)* pp 1301–4

[110] Fouladi S, Domingue F and Mansour R 2012 *CMOS-MEMS tuning and impedance matching circuits for reconfigurable RF front-ends Proc. IEEE/MTT-S Int. Microw. Symp. (Montreal, June 2012)* pp 131–3

[111] Larcher L, Brama R, Ganzerli G, Iannacci J, Margesin B, Bedani B and Gnudi A 2009 *A MEMS reconfigurable quad-band class-E power amplifier for GSM standard Proc. IEEE Int. Conf. on Micro Electro Mech. Syst. (Sorrento, Jan. 2009)* pp 864–7

[112] Iannacci J, Faes A, Mastri F, Masotti D and Rizzoli V 2010 *A MEMS-based wide-band multi-state power attenuator for radio frequency and microwave applications Proc. TechConnect World, NSTI Nanotech (Anaheim, CA, June 2010)* pp 328–31

[113] Sun J and Li Z 2016 *A broadband 3-bit MEMS digital attenuator Proc. Int. Conf. on Electron. Design ICED (Phuket, Aug 2016)* pp 442–5

[114] Iannacci J, Huhn M, Tschoban C and Pötter H 2016 RF-MEMS technology for future mobile and high-frequency applications: Reconfigurable 8-bit power attenuator tested up to 110 GHz *IEEE Electron Dev. Lett.* **37** 1646–9

[115] Iannacci J, Huhn M, Tschoban C and Pötter H 2016 RF-MEMS technology for 5G: Series and shunt attenuator modules demonstrated up to 110 GHz *IEEE Electron Dev. Lett.* **37** 1336–9

[116] Courcimault C G and Allen M G 2005 *High-Q mechanical tuning of MEMS resonators using a metal deposition-annealing technique Proc. Int. Conf. on Solid-State Sensors, Actuators and Microsyst. TRANSDUCERS (Seoul, June 2005)* pp 875–8

[117] Pillai G, Tan W S, Chen C C and Li S S 2016 *Modeling of zero TCF and maximum bandwidth orientation for lithium tantalate RF MEMS resonators Proc. IEEE Ann. Int. Conf. on Nano/Micro Engineered and Molecular Syst. NEMS (Sendai, April 2016)* pp 450–4

[118] Pacheco S, Zurcher P, Young S, Weston D and Dauksher W 2004 *RF MEMS resonator for CMOS back-end-of-line integration Proc. Top. Meet. on Silicon Monolithic Integ. Circ. in RF Syst. (Atlanta, GA, Sept. 2004)* pp 203–6

[119] Cassella C, Chen G, Qian Z, Hummel G and Rinaldi M 2017 RF passive components based on aluminum nitride cross-sectional Lamé-mode MEMS resonators *IEEE Trans. Electron Dev.* **64** 237–43

[120] Yuan Q, Luo W, Zhao H, Peng B, Yang J and Yang F 2015 Frequency stability of RF-MEMS disk resonators *IEEE Trans. Electron Dev.* **62** 1603–8

[121] Hashimoto K-Y 2009 *RF Bulk Acoustic Wave Filters for Communications* 1st edn (Norwood: Artech House) p 275

[122] Enz C C and Kaiser A 2013 *MEMS-based Circuits and Systems for Wireless Communication* 1st edn (New York: Springer) p 332

[123] Aigner R 2008 *SAW and BAW technologies for RF filter applications: A review of the relative strengths and weaknesses Proc. IEEE Ultrasonics Symp. (Beijing, Nov. 2008)* pp 582–9

[124] Koohi M Z, Lee S and Mortazawi A 2016 *Design of BST-on-Si composite FBARs for switchable BAW filter application Proc. Europ. Microw. Conf. EuMC (London, Oct. 2016)* pp 1003–6

[125] Gaddi R, Gnudi A, Franchi E, Guermandi D, Tortori P, Margesin B and Giacomozzi F 2005 Reconfigurable MEMS-enabled LC-tank for multi-band CMOS oscillator *Proc. IEEE MTT-S Int. Microw. Symp. IMS (Long Beach, CA, June 2005)* pp 141–4

[126] Cazzorla A, Sorrentino R and Farinelli P 2015 *MEMS based LC tank with extended tuning range for multi-band applications Proc. IEEE Mediterranean Microw. Symp. MMS (Lecce, Nov.–Dec. 2015)* pp 141–4

[127] Small J, Arif M S, Fruehling A and Peroulis D 2013 A tunable miniaturized RF MEMS resonator with simultaneous high Q (500–735) and fast response speed (<10–60 μs) *IEEE J. Microelectromech. Syst.* **22** 395–405

[128] Irshad W and Peroulis D 2011 *A 12–18 GHz electrostatically tunable liquid metal RF MEMS resonator with quality factor of 1400–1840 Proc. IEEE MTT-S Int. Microw. Symp. IMS (Baltimore, MD, June 2011)* pp 141–4

[129] Psychogiou D, Yang Z and Peroulis D 2012 *RF-MEMS enabled power divider with arbitrary power division ratio Proc. Europ. Microw. Conf. (Amsterdam, Oct. 2012)* pp 53–6

[130] Ocera A, Farinelli P, Cherubini F, Mezzanotte P, Sorrentino R, Margesin B and Giacomozzi F 2007 *A MEMS-reconfigurable power divider on high resistivity silicon substrate Proc. IEEE/MTT-S Int. Microw. Symp. IMS (Honolulu, HI, June 2007)* pp 501–4

[131] Ocera A, Gatti R V, Mezzanotte P, Farinelli P and Sorrentino R 2005 *A MEMS programmable power divider/combiner for reconfigurable antenna systems Proc. Europ. Microw. Conf. (Paris, Oct. 2005)* pp 141–4

[132] Marcaccioli L, Farinelli P, Tentzeris M M, Papapolymerou J and Sorrentino R 2008 *Design of a broadband MEMS-based reconfigurable coupler in Ku-band Proc. Europ. Microw. Conf. (Amsterdam, Oct. 2008)* pp 595–8

[133] Gurbuz O D and Rebeiz G M 2015 A 1.6–2.3-GHz RF MEMS reconfigurable quadrature coupler and its application to a 360° reflective-type phase shifter *IEEE Trans. Microw. Theory Tech.* **63** 414–21

[134] Ocera A, Farinelli P, Mezzanotte P, Sorrentino R, Margesin B and Giacomozzi F 2007 *Nov el RF-MEMS widely-reconfigurable directional coupler Proc. Europ. Microw. Conf. (Munich, Oct. 2007)* pp 122–5

[135] Shah U, Sterner M and Oberhammer J 2013 High-directivity MEMS-tunable directional couplers for 10–18-GHz broadband applications *IEEE Trans. Microw. Theory Tech.* **61** 3236–46

[136] De Angelis G *et al* 2008 *Packaged single pole double thruSPDT) and true time delay linesTTDL) based on RF MEMS switches Proc. Int. Semicond. Conf. CAS (Sinaia, Oct. 2008)* pp 227–30

[137] Fu D, Bey Y A, Domier C, Luhmann N C and Liu X 2015 *A Q-band RF-MEMS tapered true time delay line for fusion plasma diagnostics systems Proc. IEEE MTT-S Int. Microw. Symp. IMS (Phoenix, AZ, May 2015)* pp 131–3

[138] Van Caekenberghe K and Vaha-Heikkila T 2008 An analog RF MEMS slotline true-time-delay phase shifter *IEEE Trans. Microw. Theory Tech.* **56** 2151–9

[139] Hacker J B, Mihailovich R E, Kim M and DeNatale J F 2003 A Ka-band 3-bit RF MEMS true-time-delay network *IEEE Trans. Microw. Theory Tech.* **51** 305–8

[140] Kim M, Hacker J B, Mihailovich R E and DeNatale J F 2001 A DC-to-40 GHz four-bit RF MEMS true-time delay network *IEEE Microw. Wirel. Comp. Lett.* **11** 56–8